# Silicon Electrolyte Interface Stabilization (SEISta)

## Third Quarter Progress Report 2018

**Anthony Burrell**

National Renewable Energy Laboratory
15013 Denver West Parkway
Golden, CO 80401
Phone: (303) 384-6666
E-mail: anthony.burrell@nrel.gov


**Brian Cunningham, DOE-EERE-VTO Program Manager**

Hybrid Electric Systems, Battery R&D
Phone: (202) 586-8055
E-mail: brian.cunningham@ee.doe.gov

## Table of Contents

## Project Introduction

Silicon is a viable alternative to graphitic carbon as an electrode in lithium-ion cells and can theoretically store >3,500 mAh/g. However, lifetime problems have been observed that severely limit its use in practical systems. The major issues appear to involve the stability of the electrolyte and the uncertainty associated with the

formation of a stable solid electrolyte interphase (SEI) at the electrode. Recently, calendar-life studies have indicated that the SEI may not be stable even under conditions where the cell is supposedly static. Clearly, a more foundational understanding of the nature of the silicon electrolyte interface is required if we are to solve these complex stability issues. A new multi-lab consortium has been formed to address a critical barrier in implementing a new class of materials used in lithium-ion batteries that will allow for smaller, cheaper, and better performing batteries for electric-drive vehicles. This consortium, named the Silicon Electrolyte Interface Stabilization (SEISta) project, was formed to focus on overcoming the barrier to using such anode materials. Five national laboratories, are involved:  NREL, ANL, LBNL, ORNL, and SNL.

The SEISta project was developed to specifically tackle the foundational understanding of the formation and evolution of the solid electrolyte interphase on silicon. This project will have as its primary goal an understanding of the reactivity of the silicon and lithiated silicon interface with the electrolyte in lithium-ion systems. It consists of researchers from multiple national laboratories (ANL, SNL, ORNL, LBNL, and NREL) working toward clear unified goals.  The Silicon Deep Dive team which is focused upon the science and technology barriers in functional electrodes is a critical partner in this work.  Many of the researchers are shared between both teams and we hold joint meetings to ensure effective communication between the teams.

*The current goals of SEISta are:*

Quarter 1 Milestone:

Have completed the selection and characterization (XPS, SIMS, IR, and Raman), including determination of the surface termination chemistry and impurity levels, of the SEISta model research samples to be used by all members of the team in FY18. (100 % complete)

Quarter 2 Milestone:

Have characterized (XPS, SIMS, IR, and Raman) the surface chemistry and composition of the SEISta model research samples after contact with the electrolyte, before cycling, including the nature of the electrolyte decomposition products.  (100% complete)

Quarter 3 Milestone:

Completed characterization (electrochemistry, IR and Raman) of the early stage silicon electrolyte interphase formation on the SEISta model research samples, specifically by establishing and demonstrating a procedure for quantitatively measuring the solubility of SEI on silicon surfaces. (80% complete)

Quarter 4 Milestones:

Established and demonstrated a procedure for measuring the growth rate of silicon SEI components at fixed potentials and during cycling.

Have determined how the physical properties of the silicon electrolyte interface are influenced by the nature of the silicon surface on the SEISta model samples.

## Approach

The SEISta team works to ensure that protocols for sample preparation, experimental design and implementation, as well as data reporting are consistent across the whole team. Each laboratory is working toward the same set of quarterly milestones using its own specific talents and capabilities in a concerted effort with the other team members. This joint focus results in multiple researchers interacting to produce and analyze data to ensure that individual experimental variations will not lead to erroneous results. Critical to the success of this effort is the use of standard samples that can be shared by all parties. In the first FY, a round-

robin sample test was established to ensure that data could be duplicated at the different laboratories by different researchers. In addition to weekly whole-team video presentations, we have held on-site face-to-face meetings each quarter for all team members, and other interested parties, to brainstorm and sort out issues with existing experiments and jointly develop new experimental plans.

The outcomes from FY17 indicated that the nature of the silicon starting materials has major implications for the formation and evolution of the SEI.  This is most clearly seen in the inherent chemical reactivity of the silicon materials with electrolytes before electrochemistry.  Much of our focus for FY18 will be in looking at the initial chemistry of the silicon on contact with electrolytes.  This will then lead to an understanding of how the electrode electrolyte interface changes upon applied voltage and how the SEI forms and evolves.

## Objectives

The critical issues SEISta is attempting to determine are:
- What are the properties of the lithiated silicon electrolyte interface?
- What is the Silicon SEI actually made of and what reactions are contributing to it?
- How fast does the Silicon SEI grow?
- Does it stop growing?
- Is it soluble?
- Can it be stabilized?

For this quarter the team focused on three broad tasks:

**Materials Standardization** – This task is critical to the development and deployment of standardized samples and experimental procedures across the team.  We will continue to provide full characterization to any new sample that is to be used for SEI studies to ensure reproducibility and full understanding of the material. This Quarters work has focused upon the development of new oxide coatings and methods to control the thickness and density of oxide samples.  In addition work on the silicon nano-particles has made progress with the enhancement of the materials collection and handling system in the plasma reactor.  *While this work dominated the early part of the project and is still critical to the its success, it is now only a minor part of the work and this is reflected in the relative balance of this quarterly report. .*

**Model Materials Development and Characterization** – The nature of the electrode-electrolyte interaction in silicon electrodes is at the heart of the formation and stability of the SEI.  The inherent chemical reactivity of silicon with common electrolytes has been a focus for this team and will be a primary focus moving to quarter 2.  The synthesis of well-defined silicon nanoparticles and the different chemical markups of lithiated silicon surfaces is being probed by preparing model compounds and thin films that may/can exist in silicon anodes.  Lithium silicides, silicates, and other inorganic material (LiF, $Li_2O$) are being prepared and their reactivity with electrolytes is being determined.  These materials also act as standard spectroscopy samples for the researchers who are looking at the formation of the SEI on different silicon materials.

**SEI Characterization** – The overall objective for SEISta is to understand the nature and evolution of the SEI on silicon anodes. The materials standardization and model compounds will enable the researchers to systematically investigate the formation of the solid electrode interphase using a wide variety of the spectroscopy techniques, from different optical, microscopy, and electrochemistry to determine how the SEI forms based upon the nature of the silicon surface, and how it evolves over time. This section of work will continue to grow in scope as we move beyond the sample characterization phase of the project and on to the understand the nature and evolution of the SEI. *This part of the project now represents the bulk of the work and as such this quarterly report is largely reporting on work leading to this outcome.*

## Milestone Quarter 3 FY18: Silicon Electrolyte Interface Stabilization (SEISta)

**SEISta Team**

### Background

The overall objective of the SEISta project is to better understand the formation and evolution of the solid electrolyte interphase (SEI) on silicon anodes. Silicon is a viable alternative to graphitic carbon as an electrode in lithium-ion cells and can theoretically store >3,500 mAh/g. However, lifetime problems have been observed that severely limit its use in practical systems. The major issues appear to involve the stability of the electrolyte and the uncertainty associated with the formation of a stable solid electrolyte interphase (SEI) at the electrode. Recently, calendar-life studies have indicated that the SEI may not be stable even under conditions where the cell is supposedly static. Clearly, a more foundational understanding of the nature of the silicon electrolyte interface is required if we are to solve these complex stability issues. A multi-lab consortium has been formed to address a critical barrier in implementing a new class of materials used in lithium-ion batteries that will allow for smaller, cheaper, and better performing batteries for electric-drive vehicles. This consortium, nicknamed the Silicon Electrolyte Interface Stabilization (SEISta) project, was formed to focus on overcoming the barrier to using such anode materials. Five national laboratories, led by the National Renewable Energy Laboratory (NREL), are involved: NREL, as well as Argonne (ANL), Lawrence Berkeley (LBNL), Oak Ridge (ORNL), and Sandia National Laboratories (SNL). The third quarter milestone for SEISta in FY18 was:
*Completed characterization (electrochemistry, IR and Raman) of the early stage silicon electrolyte interphase formation on the SEISta model research samples, specifically by establishing and demonstrating a procedure for quantitatively measuring the solubility of SEI on silicon surfaces.*

### Results

This objective was 80% completed, as we have only obtained qualitative data on the dissolution due to equipment issues and there are differences in the SEI behavior depending on electrode voltage. The differences observed between the SEI stability at different voltages will be resolved and the objective will be complete by the end of Q4

This milestone requires the efforts and interactions of all team members and the results are described in the individual report sections below along with work related to other FY18 milestones. This short overview covers some of the points that lead to the (almost) completed milestone, which are:

1. Establish protocols for the development of samples and analysis of the SEI.
2. Utilizes multiple spectroscopy techniques to characterize the early stage SEI. (diagnostic studies)
3. Determine the solubility of the SEI on silicon surfaces.

**1) Protocol Development**
The first step was the development of procedure for measuring the solubility of the SEI on silicon surfaces. The current electrochemical procedure to determine SEI stability and correlate this with thickness and stability. The initial parameters and procedures are as follows:

*Manufacturing of Si model electrodes*

**The principle for selecting the samples is to decouple lithiation current versus corrosion/ passivation current. <u>All Si electrodes must yield reproducible results under the same testing conditions. Therefore consistency of the key physico-chemical parameters of Si electrodes such as thickness, crystallinity, Si surface orientation is essential for the success of this research thrust.</u>**

Amorphous (a) Si thin film on a copper (Cu) foil. *a*-Si thin film with a thickness of 50 nm will be prepared by radio frequency magnetron sputtering at Oak Ridge National Laboratory

Electrochemically pretreated Si wafer samples. These electrodes consist of *a*-Si thin layer (~50nm) at the top of the Si wafer produced by controlled lithiation/delithiation of the top layer of the Si wafer. This sample design is based on an assumption that only a-Si top layer undergoes lithiation whereas the underneath bulk crystalline (*c*) Si remains inactive during the sequential electrochemical cycling and/or chronoamperometry experiments. Prior to using this set of samples a proof of concept needs to be demonstrated.

Composite Si electrodes made with *c*-Si nano-particles and polymer binder (no conductive carbonaceous additives). The electrode consists of a monoparticulate thin-film produced by drop casting/laminating/spin-coating Si-binder slurry on the Cu current collector.

*Electrochemical testing*.

To evaluate the passivating properties of Si at various potentials a series of preliminary chronamperometry measurements will be carried out over a prolonged period of time. The current profile and the total amount of charge consumed by the electrolyte reduction processes with regard to the known reversible lithiation/delithiation charge will be used to assess (non-)passivating properties of the SEI layer on the Si electrode.

The pristine model Si electrode will be charged/discharged galvanostatically (5uA/cm$^2$ for a-Si electrodes) till the electrode potential reaches 1.5, 0.5, 0.3, 0.05, 03, 0.5 and 1.5 V followed by polarization at those potentials for >40 hours. A similar sequence of chronoamperometric measurements will be carried out during the 2nd and 3rd scan (see Figure 1). The current will be monitored and recorded during long-term constant potential polarization.

Swagelok three-electrode T-cells should be used to carry out all electrochemical tests. Li foil (Alfa Aesar part number 10769) will be used as counter and reference electrodes. Two separators soaked with Gen2 electrolyte will be used to assemble the cell.
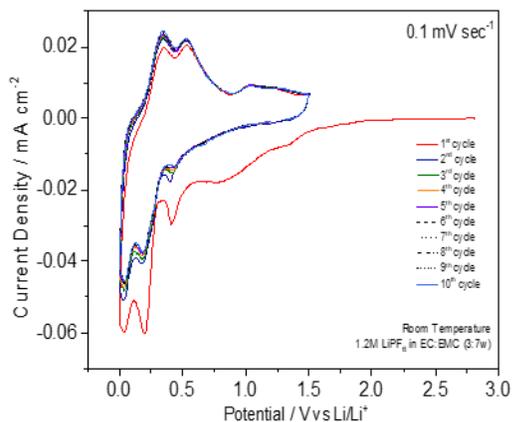


**Figure 1. Typical CV plots of the a-Si thin film electrode. The cut-off potential for the electrochemical testing protocol are 1.5V, 0.5V, 0.3V and 50 mV.**
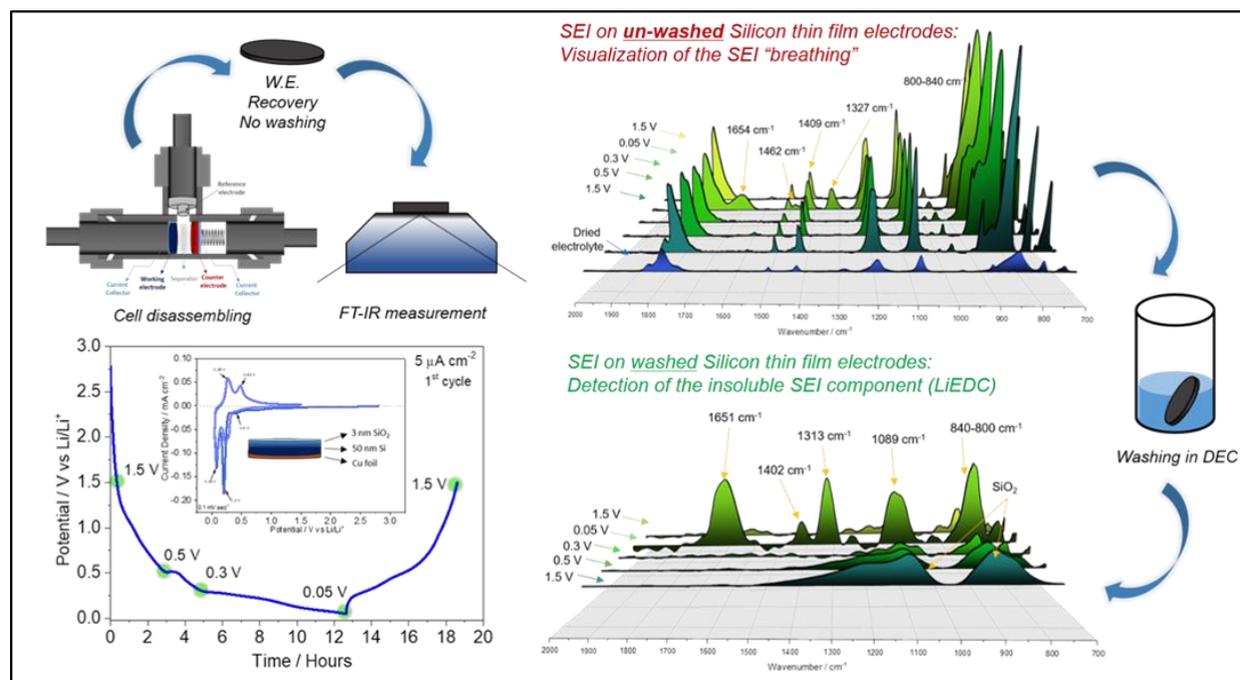
Considering that these measurements will most likely generate small currents (<1 pA) over a prolonged period of time it's recommended that only high precision potentiostats are used (standard battery cyclers are inappropriate to perform these measurements). The electrochemical cell should be shielded in a Faraday cage during the test. Proper cable shielding and grounding is essential to reduce signal noise. Please refer to your potentiostat manual for technical details.

## 2) Diagnostic studies

One reason we have not completed this objective to 100% is while we see data that is consistent with SEI dissolution we have not quantified the dissolution. When silicon samples with an oxide layer are cycled to voltages where lithiation of the silicon is certain there is evidence that components of the SEI are soluble in the electrolyte, as shown in Highlight 1. However, when the potential is held to voltages above where lithiation of the silicon occurs ((<400 mV) the SEI appears to be growing but when the voltage gets to 115mV the SEI starts losing thickness seen in highlight 2. In addition, we have observed a complication in that silicon oxide interface maybe reacting to produce soluble components which complicates things even more see Highlight 3. Over the next quarter we will *quantify* the dissolution process that appear to be occurring thin the Gen-2 SEIs on silicon.

Highlight 1

Electrochemical results from chronoamperometric tests will be used to assess the (non-) passivating properties of the SEI layer on the silicon model electrodes in Gen-2 electrolyte. The corresponding in situ and ex situ diagnostics measurements of the Si electrodes and electrolytes after the tests will be conducted with e.g., FTIR, NMR, XAS, XPS, GCMS and NMR to correlate the observed electrochemical behavior with the thickness, composition and structure of the SEI layer and possible presence of soluble compounds in the electrolyte. While we have carried out extensive work in the diagnostics we have not yet quantified the solubility and this work will continue through Q4.



Electrochemical and spectroscopic characterization of the silicon electrolyte interphase formation on the Si thin film SEISta model samples, with and without oxides overlayers, has been completed.

For all the investigated samples, we detected a dynamic growth and disappearance of the passivating surface film, suggesting the oxide layer does not affect the interfacial chemistry significantly. This fundamental observation represents a step forward the understanding of the inherent non passivating behavior of silicon electrodes. A qualitative detection of the chemical compounds most likely responsible of the "breathing" effect of the surface film has been successfully reached, thus enabling the correlation of the formation and disappearance of LiEDC, but also to P-F containing species, to the stability of the SEI .

The developed protocol for ex-situ investigation of the silicon SEI at different state of charge, enabled the identification of the stability in terms of solubility of the compounds deposited on the silicon surface. All the

SEI components are found to be soluble with the only exception of LiEDC, thus confirming the fundamental role of LiEDC in the silicon SEI stability.

Highlight 2

The early stage SEI was probes several ways using controlled materials and electrochemical methods. Early stage solid electrolyte interphase (SEI) formed on silicon wafers from various cycling and resting conditions was characterized with scanning probe microscopy (SPM) to investigate morphological and structural development during cycling and resting. Total SEI thickness was shown to increase during resting, suggesting that the SEI has limited solubility in electrolyte (a result that is contradiction to the washing experiments), and additional deposition of electrolyte decomposition products takes place during resting. Scanning transmission electron microscopy (STEM) and SPM characterization of Si wafers cycled with greater current densities and cutoff potentials showed SEI to develop at thicknesses of tens of nanometers in the first lithiation and delithiation. These results suggest that SEI is generally insoluble in Gen2 electrolyte (EC:EMC (3:7 by wt.) + 1.2M LiPF6) as well as DMC (used to rinse the wafer samples after cell disassembly).

Early stage SEIs, formed under highly constrained cycling cutoff voltages (<400 mV, with little to no lithiation/delithiation occurring) on native oxide Si wafers were analyzed with atomic force microscopy (AFM) in tapping mode and scanning spreading resistance microscopy (SSRM) in contact mode. Surface morphology of these SEIs were measured with AFM to establish trends for root mean square (RMS) surface roughness. SSRM was employed to measure total SEI thickness and compare electronic resistivity of superficial regions of SEI. Dozens of samples were characterized to determine the effects of varying cutoff voltage, cell resting, and total number of cycles. Trends for early-stage SEI formation in Gen2 electrolyte can be seen in the table below.

<p align="center">Table-1: Early-Stage SEI Development</p>

| Effect of | Surface Roughness | SEI Thickness | SEI Surface Resistivity |
|---|---|---|---|
| Resting (No rest vs 50 Hours) | Decreased Roughness (3.3 nm → 1.8 nm) | Increased Thickness (2.8 nm → 3.4 nm) | Less Resistive SEI ($10^9\ \Omega \cdot cm \rightarrow 10^6\ \Omega \cdot cm$) |
| Higher Cutoff Voltage (115 mV vs. 400 mV) | Decreased Roughness (8.0 nm → 3.3 nm) | Decreased Thickness (2.8 nm →1.5 nm) | Less Resistive SEI ($10^9\ \Omega \cdot cm \rightarrow 10^5\ \Omega \cdot cm$) |
| Increased Number of Cycles (26 vs 48) | Decreased Roughness (3.3 nm → 1.25 nm) | Increased Thickness (2.8 nm → 3.5 nm) | More Resistive SEI ($10^9\ \Omega \cdot cm \rightarrow 10^{10}\ \Omega \cdot cm$) |

Highlight 3

The nature and stability of the interface between the silicon and the SEI is also under investigation. We have created model systems of lithium silicates of varying compositions, and have studied their stability and evolution over time using various techniques, including ATRIR, XPS, SEM/FIB, and EIS. From the ATRIR data, we have observed that the higher the lithium concentration in the starting model film, the faster the film appears to both change structure and to generate lithium alkyl carbonates, possibly by accelerating the decomposition of the electrolyte. From XPS depth profiling over time, we have seen significant increases in how quickly the starting surface films are penetrated by fluorine from the electrolyte, and also that increasing amounts of lithium in the film causes restructuring of the film (whereas films that do not contain lithium are very slow to see this behavior). Finally, EIS data shows that both double layer and interfacial resistance undergo slow changes initially when exposed to electrolyte (in SiO2 at room temperature), but that abrupt changes in these values are observed after several days of incubation in electrolyte. All of these methods allow for the quantization of both composition and temporal effect on electrolyte exposure against varying compositions of silicates, and have observed structural and compositional changes which may indicate the dissolution or restructuring of the SEI on Si surfaces.
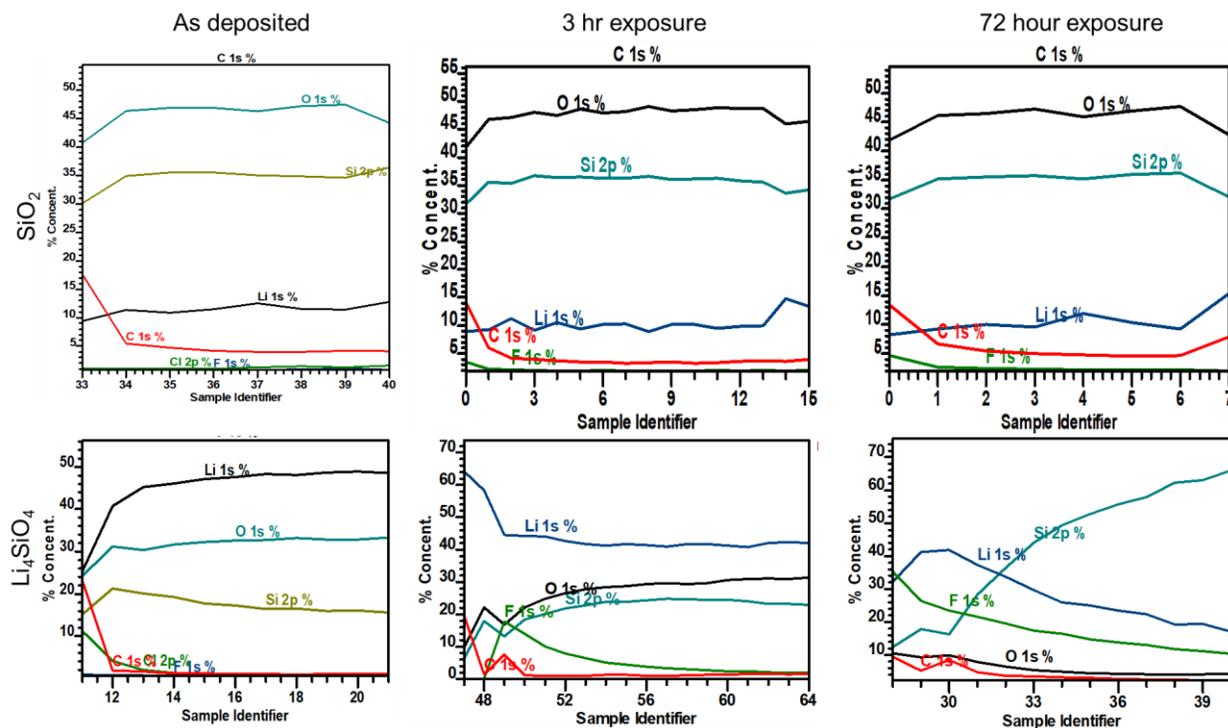
Figure 3: Depth profile XPS data for SiO2 (top) and Li4SiO4 (bottom) coated samples as deposited (left), after 3 hours of electrolyte exposure (middle) and after 3 days of exposure (right). The existing of Li starting in the silicate dramatically affects how quickly the films change composition, and the admission of fluorine into the films, along with redistribution of oxygen, Li, and Si.

**3.    Determine the solubility of the SEI on silicon surfaces.**
While the overall theme of the data collected for this milestone indicates that the SEI or components of the SEI that are soluble in the electrolyte, more work is required to both quantify the amount of and nature of the soluble species.  This will continue through Q4.

## Conclusions

The milestone was 80% completed we have yet to quantify the solubility of SEI on silicon surfaces and we still have some discrepancy in the results obtained across the teams. Qualitatively we have evidence for both solubility of the SEI in the Gen-2 electrolyte and for limited stability of the silicon surface. We will be working on understanding the differences between these results in the next quarter to come up with a clear conclusion and complete this milestone.

## Materials Standardization: Electrochemical Testing of Silicon Wafer Anodes – Corrosion Instrumentation (NREL)

Manuel Schnabel (NREL), Matt Page (NREL), Chunmei Ban (NREL), Paul Stradins (NREL)

## Background

Polished silicon wafers provide the most controlled silicon material with which to study the fundamental processes occurring during the lithiation of silicon from an electrolyte. Among these are not only the

capacity and the cycling behavior, but also the retention of charge at a high state of charge, at potentials where no lithiation/delithiation ought to occur. In the following, we outline improvements to our instrumentation that will allow us to monitor small leakage or corrosion currents that occur at such potentials.

## Results

**Measuring background currents** (electrolyte reduction or anode corrosion) at voltages where no lithiation/delithiation takes place can require the measurement of very small currents. Last quarter, we had built a Faraday cage to reduce background currents but had found that it only decreases the noise of a chronoamperometric measurement across a 10 MΩ resistor from ~4nA to ~2nA. When the sampling time is increased from 10ms to 500ms, noise is ~1 nA irrespective of whether the Faraday cage is used, which is attributed to the inherent limitations of the standard electrometer hardware in our cycling station.
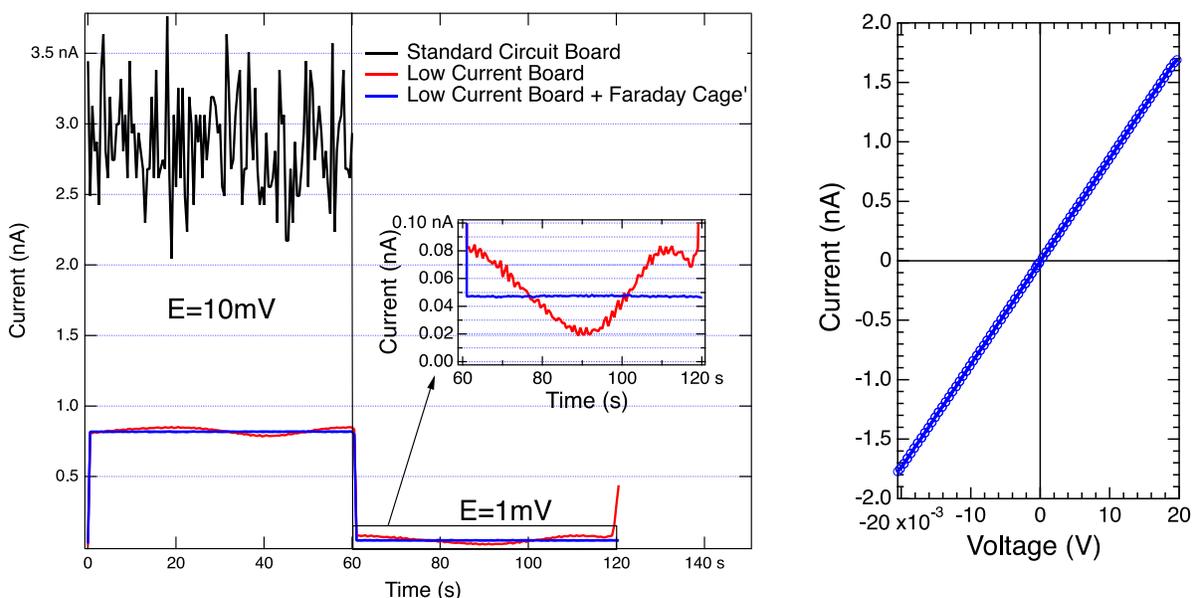


Figure 1: Left: chronoamperometric measurement at 10mV and 1mV across a 10 MΩ using the standard circuit board, a low current board, and a low current board with a Faraday cage for shielding. Right: cyclic voltammetry measurement of same resistor from -20mV to +20mV, using low current board and Faraday cage.

To improve the performance of our setup, we ordered a low-current circuit board from the cycling station manufacturer and installed it in our setup. As can be seen in Figure 1(left), this greatly reduces the noise in the measurement, but an unshielded measurement introduces oscillations in the chronoamperometric curves (see inset of Fig. 1(left)). Combining the low-current circuit board with a Faraday cage eliminates these oscillations and reduces noise to only ~1pA, improving on the prior noise levels by three orders of magnitude. As can be seen in Fig. 1(right), excellent linearity is maintained when performing cyclic voltammetry of a resistor at low voltages and currents. This current range is relevant for accurately studying background reactions: assuming an anode area of $1cm^2$, a background current of 1 nA, which standard electronics cannot detect (but the current one can, with 3 orders of magnitude over the 1 pA noise), corresponds to 0.01 mAh/$cm^2$ per year. Thus, our new capability will allow accurately measuring backcground reaction currents that have meaningful impact on the calendar life of Li ion batteries.

## Conclusions

The electronics of our cycling station have been upgraded to permit measurement of currents down to $10^{-12}$ A. This will enable us to accurately measure small background or corrosion currents on cells in the coming quarter.

# Model Materials Development and Characterization: Chemical and Electrochemical Reactivity of Plasma-Synthesized Silicon Nanoparticles

Bertrand Tremolet de Villers, Gregory Pach, Nathan Neale (NREL)

## Background

One of NREL's tasks explores plasma-synthesized silicon nanoparticles (Si NPs) as model systems for $Li_xSi$ anodes. Such plasma-prepared Si NPs are valuable since they feature hydrogen-passivated surfaces and a high surface area resulting from their <10 nm diameter that makes them well suited for chemical reactivity studies using Fourier transform infrared (FTIR) spectroscopy and quantitative off-gassing analysis. These reactivity studies are relevant for understanding (1) early-stage SEI layer growth as well as (2) individual SEI component chemical stability. In FY17 and early FY18, we prepared several ~100 mg batches of ~7 nm diameter Si NPs for chemical reactivity studies. Making larger diameter (10–200 nm) Si NPs and at a greater scale (>>100 mg) as well as extending chemical reactivity to electrochemical reactivity are key objectives in FY18.

## Results

In Q3 FY18 we operated at full staffing that resulted in significant progress toward year-end goals:

1. Expand existing RF plasma reactor to produce larger Si nanoparticles (NPs) and at greater scale
   a. Subtask FY18 Q4 Milestone: 30–50 nm diameter and 0.5–1.0 g (per basket)
2. Use Si NPs as high surface area model systems for:
   a. Chemical reactivity studies
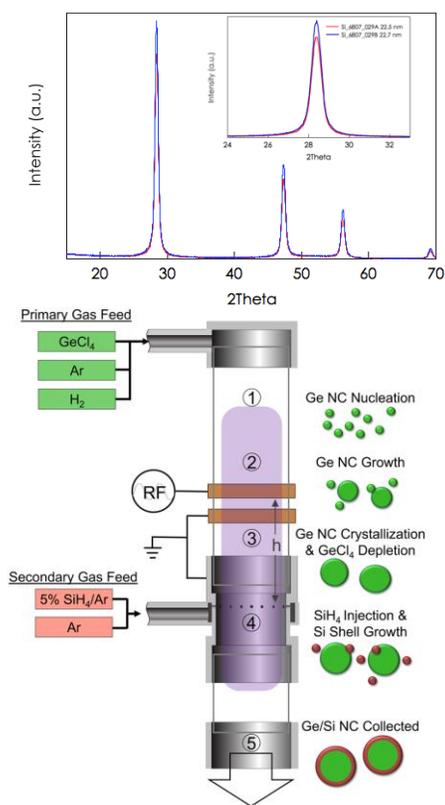   b. Electrochemical reactivity studies

Tasks 1 & 2 ultimately will enable the evaluation of plasma-synthesized Si NPs in batteries both with and without surface modifications. Modifications could include both molecular functionalization (e.g., alkoxides, fluorinated hydrocarbons/alkoxides) or inorganic coatings (e.g., oxides, nitrides, carbides). In FY18 we are establishing the baseline chemical and electrochemical reactivity of plasma-grown Si NPs. Essential to these tasks is the ability to scale up our process to battery-relevant quantities as well as sizes an order of magnitude greater than we had produced prior to the SEISta project.

Some effort in Q3 was spent exploring the plasma growth conditions, and those activities will continue for the duration of FY18. In Q2, we established that ~18 nm diameter Si NPs were achieved by an argon plasma containing 17% silane gas ($SiH_4$) run at ~6 Torr pressure and a plasma power density of >2 W $cm^{-3}$. In Q3, we have explored just a small fraction of the pressures (ca. 1–100 Torr) and flow rates (ca. 3–500 sccm $SiH_4$) theoretically accessible using our reactor system. This is because have found that there are practical limitations on these parameters relating to pumping speed and pressure drop across a clogging particle filter that limit our ability to achieve a significantly wider range of pressures and flow rates. We are devising solutions around this problem including a ratcheting restrictive flow orifice (RFO) that should enable us to dynamically tune the system conductance (an engineering term used to describe the impedance to pumping) as the abundance of Si NPs produced clog the mechanical filter – yes this is a good problem to have to tackle!

As another workaround these limitations, in Q3 we have additionally devised experiments where we have used a secondary gas injection system to add additional silicon material onto the surface of our Si NPs. This strategy previously has been applied to growing core-shell Ge@Si NPs by first producing Ge NPs in the

upstream plasma, and then downstream during the so-called afterglow region (where the plasma is still active but much less energetic) injecting a secondary gas (here, $SiH_4$) to grow a Si shell on a Ge core. The basic schematic is shown in Fig. 1. In our experiments, we used our well-established 10% $SiH_4$ in helium carrier gas mixture in our primary Si NP growth process and added 100% $SiH_4$ as the secondary gas injection. This process allowed us to prepare 22.5 and 22.7 nm diameter Si NPs in our first two attempts. Note also that our typical size determination based on Scherrer analysis XRD spectra peak width is likely a lower limit since in this size regime particles become indistinguishable from bulk due to linebroadening effects. We have lined up our characterization team and plan to partner with Dr. Mowfak Al-Jassim's efforts to characterize Si NP size through TEM imaging that will provide a more accurate measure of the Si NP diameter. Still, if we assume the lower-limit 22.6±0.1 nm diameter found via XRD is correct, these Si NPs represents a 4.3 nm diameter increase and an impressive 98% volume increase over the 18 nm diameter NPs achieved in Q2FY18.

As an added benefit of this secondary 100% $SiH_4$ gas injection, we additionally achieved a dramatic increase in the scale of our process and were able to collect ~0.4 g of Si NP powder in just 15 min of reactor run time. Without the secondary gas injection, far longer times on the order of 1–2 h are required to generate this much material. We are confident based on this progress that additional experimental refinements will



allow us to achieve our Q4 Milestone of 30–50 nm diameter Si NPs at a scale of 0.5–1.0 g per run.

Figure 1. Top: Schematic of secondary gas injection setup that enables additional material to be added on top of a primary NP core. From reference 1. In our work, this strategy has been used to grow 22.6±0.1 nm diameter Si NPs (Bottom: XRD spectra).

Next, we have continued to work with partners on manuscripts detailing Task 2a: Chemical reactivity studies of SEISta model samples including Si NPs, $SiO_x$ NPs, and $Li_2SiO_3$ and $Li_4SiO_4$ particles. In late April we received data from SEISta partner Prof. Kristin Persson at UC Berkeley on density functional theory (DFT) calculations on the vibrational modes of various chemical species that corroborate our experimental results from Q4FY17. We are working on a manuscript with her and her team and expect to submit this publication for peer review in Q4FY18.

In Q3, we additionally have teamed with SEISta partner Dr. Zhengchen (John) Zhang at ANL to send him samples of our plasma-prepared Si NPs for surface chemistry studies. Dr. Zhang and his team have already demonstrated functionalization of our Si NPs to prepare $^*Si–(EO)_3–OCH_3$, where $^*Si$ denotes a Si NP surface Si atom and EO = ethylene oxide. Future work on exploring the effects of this surface chemistry on the performance in battery electrodes in planned for Q4FY18.
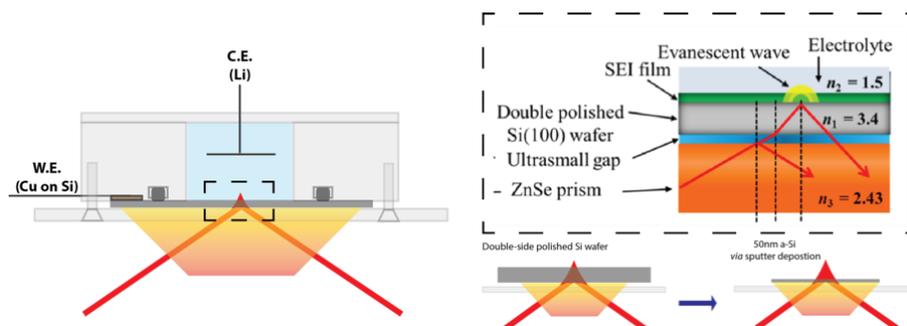


**Figure 2. Left: Schematic of in operando ATR-FTIR cell for spectroscopically interrogating SEI chemical components under electrochemical bias in electrolyte; Top Right: Detail of active area from reference 3; and Bottom Right: Two alternative setups for examining various SEISta samples.**

Finally, we have accomplished our self-assigned Q3FY18 Milestone: Complete design and acquisition of in operando attenuated total reflectance Fourier transform infrared (ATR-FTIR) cell(s) with electrochemical interface, and associated hardware. As shown in Fig. 2 and as described in our Q1- and Q2FY18 reports, we have worked with Dr. Phil Ross (LBNL) given his extensive prior work in this area[2,3] to ensure the validity of the design. We have developed a custom air-free cell that allows us to access a Si wafer surface electrochemically, and have performed initial experiments using this ATR-FTIR-electrochemical setup. In the first setup, a double-sided polished Si wafer is placed on top of the ZnSe ATR crystal. There are several challenges with this approach: (1) Si does not provide a perfect refractive index match to ZnSe, (2) the "ultrasmall gap" between the ZnSe ATR crystal and Si substrate pictured in Fig. 2 is difficult to minimize, and (3) passing the IR beam through a Si wafer attenuates the signal. Challenges (1) and (2) are manageable with further optimization, and so we have been focused on mitigating challenge (3) by optimizing the Si wafer to balance the competing trade-off between resistivity and IR transmittance. Lightly-doped Si wafers with carrier densities $\sim 10^{15}$ cm$^{-3}$ provide good IR transmission, however are somewhat resistive (1–5 $\Omega$ cm). In contrast, highly-doped Si wafers with carrier densities $\sim 10^{18}$ cm$^{-3}$ provide poorer IR transmission but are much less resistive (1–5 m$\Omega$ cm). The wafer thickness also is an important factor, with 1 mm thick wafers offering poorer transition but better structure stability than thinner (100–300 $\mu$m thick) wafers.

Given these challenges, we are also exploring a 2nd alternative setup in parallel by depositing SEISta model samples (e.g., 50 nm thick Li$_x$Si) *directly* onto the ZnSe ATR crystal. We have worked with Dr. Andriy Zakutayev who has deposited a 50-nm thick amorphous Si layer on top of the ZnSe ATR crystal and we are in the process of conducting the first experiments on this new setup.

## Conclusions

Key findings in this reporting period are:
- Scale-up of Si NPs is in progress, with reasonable yields (~0.4 g per basket in just a 15-min production run) and increased size (22.6 nm diameter) and volume (98% increase cf. 18-nm diameter Si NPs) over our Q2FY18 samples.
- Progress on our in operando ATR-FTIR-electrochemical setup is somewhat slower than expected, and so we have devised a parallel alternative setup that will allow additional unique experiments on SEISta model samples.

Future FY18 efforts will be devoted toward continuing to explore the parameter space to increase Si NP sizes and yields further, as well as to further refinement of our in operando ATR-FTIR-electrochemical instrument.

## References

1. Hunter, K. I.; Held, J. T.; Mkhoyah, K. A.; Kortshagen, U.R. *ACS Appl. Mater. Interfaces* **2017**, *9*, 8263.
2. Shi, F.; Ross, P. N.; Zhao, H.; Liu, G.; Somorjai, G. A.; Komvopoulos, K. *J. Am. Chem. Soc.* **2015**, *137*, 3181.
3. Shi, F.; Ross, P. N.; Somorjai, G. A.; Komvopoulos, K. *J. Phys. Chem. C* **2017**, *121*, 14476.

# Model Materials Development and Characterization: Inherent Reactivity Studies of Lithium Silicides

**Baris Key (ANL), Binghong Han (ANL), Fulya Dogan (ANL), Chen Liao (ANL), Jack Vaughey (ANL)**

## Background

One of the core problems associated with Li-Si chemistry in Li-ion batteries is the inherent reactivity of the lithium silicides, the active material that forms upon the lithiation. These phases can react with almost all battery components such as binders, electrolytes, additives and impurities such as moisture and air which cause major columbic losses and loss of lithium.

## Results

A synthetic and characterization effort was undertaken to prepare key model compounds in the Li-Si phase diagram. In previous reports, X-ray diffraction and Solid State Magic Angle Spinning (MAS) NMR spectroscopy have been used to qualitatively and quantitatively study the potential reactions between the lithium silicides model compounds and different electrolyte components, such as EC, EMC, triglyme and FEC. It is found that compared with EC and EMC, triglyme solvents lead to less $^7$Li and $^{29}$Si MAS NMR shifts after mixed with the $Li_7Si_3$ model compounds (reported in Q1 and Q2 FY'18), which according to the previous NMR study (1,2), representing less delithiation of lithium silicides and better chemical stability in contact with the charged Si anodes. Meanwhile, it is interesting to discover that FEC also showed only slight reactions after mixed with the $Li_7Si_3$ with no LiF formation, contrary to the common belief that FEC defluorination reaction would be prevalent in the presence of lithium silicides (reported in Q2 FY'18). The FEC results suggested either $Li_7Si_3$ of about 0.3-0.4 V vs. Li is not reducing enough and/or a flow of electrons is also required for FEC passivation reaction.

To test the above hypothesis, new lithium silicide compound with higher Li contents (i.e. representing lower charging potential, $Li_{13}Si_4$) were synthesized, and then mixed with FEC and other solvent. Because of the excess Li in the reaction container to mitigate Li-loss the newly synthesized lithium silicide was instead identified as $Li_{22}Si_5$ according to its $^7$Li MAS NMR spectrum shown in Figure 1a, which corresponds to about 0.05-0.1 V vs. Li (3,4). The $^7$Li and $^{29}$Si MAS NMR results of the mixture of $Li_{22}Si_5$ and different electrolyte solvents, including EC, FEC and triglyme, are shown in Figure 1. After mixing with FEC or EC, the main $^7$Li peak of $Li_{22}Si_5$ at ~75 ppm shifted by ~4 ppm, indicating the lithium loss caused by the reaction between $Li_{21}Si_5$ and FEC/EC. Meanwhile, unlike the minor $^7$Li and $^{29}$Si NMR shifts previously observed after mixing $Li_7Si_3$ with triglyme (reported in Q2 FY'18), this time clear positive peak shifts and notable broadening were observed after mixing $Li_{21}Si_5$ with triglyme. Such obvious peak evolution indicated that although triglyme might be relative stable when in contact with the slightly-charged Si anode, it could react with the Si anode charged to lower voltages. It must be noted that $Li_{22}Si_5$ NMR shifts are non-diamagnetic and the shift mechanism is due to conduction band electrons at the Fermi level, i.e. Knight shift, therefore a simple interpretation of shift changes to higher or lower frequencies cannot be easily made as in the case of $Li_7Si_3$. Still, the results indicate a bulk reaction and can partially explain our earlier observation that in half-cell tests using 1M LiTFSI in triglyme as the electrolyte, the capacity of Si anodes dropped faster over cycles compared with the Gen2 + 10% FEC electrolyte (reported in Q2 FY'18). In addition, in the $^7$Li MAS NMR spectra shown in Figure 1a, a clear diamagnetic $^7$Li peak around 0 ppm (could be ascribed to LiF, $^{19}$F NMR pending) appeared after mixing $Li_{21}Si_5$ with FEC. This means our earlier observation that the mixing of FEC and $Li_7Si_3$

causes no LiF formation presumably due to $Li_7Si_3$ not being reducing enough. The above results suggest triglyme may not stable/passivating enough alone for high Li content $Li_xSi$ . New carbonate electrolyte formulations and non-carbonate are still required to further improve the coulombic efficiency, which will be the focus of new electrochemical tests in the next quarter.
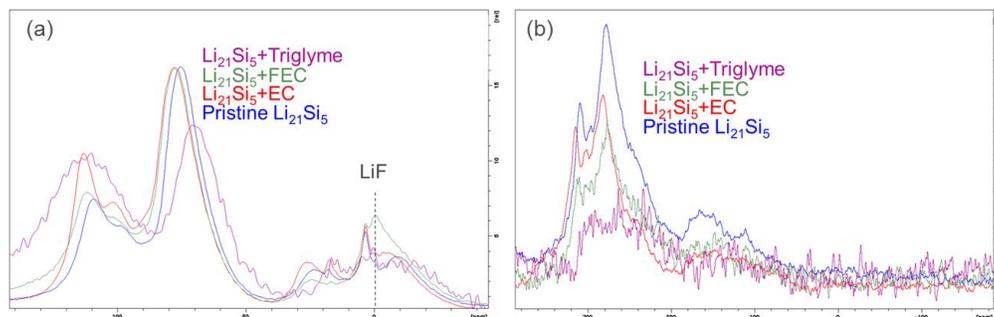


**Figure 1. (a) $^7$Li and (b) $^{29}$Si in-situ solid state MAS NMR for $Li_{22}Si_5$ and different electrolyte solvents. ANL, unpublished results.**

Beside model compound experiments, we also measured the chemistry evolution of the Si anodes in half cells previously reported, cycled between 0.01-1.5 and 0.05-1.5 V vs. Li respectively for 15 cycles using 1 M LiTFSI in trigylme as the electrolyte, as shown in Figure 2. The $^{13}$C NMR results indicated that the reaction between triglyme and charged Si anodes could cause the degradation of triglyme into ethylene glycol and cleaved aliphatics.
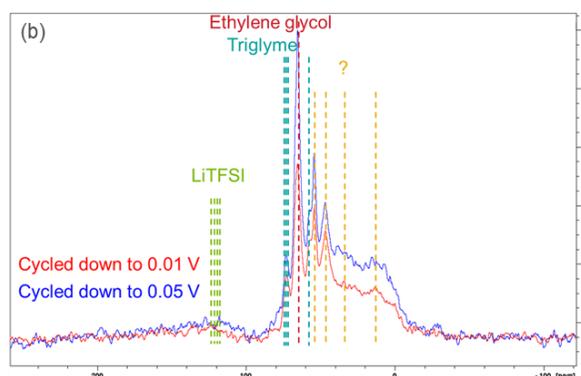


**Figure 2. $^{13}$C solid state MAS NMR for post-electrochemistry Si loose-powder anodes after cycling between 0.01-1.5 and 0.05-1.5 V vs. Li respectively for 15 cycles, using 1 M LiTFSI in trigylme as the electrolyte. ANL, unpublished results.**

## Conclusions

Quantification of the reactivity of $Li_{22}Si_5$ vs. EC, FEC, and triglyme showed that more reducing lithium silicides can trigger new reactions that may lead to the defluorination of FEC and the degradation of triglyme, which could explain the fast capacity fading observed in the half-cell tests using glyme-based electrolytes last quarter. Initial post-electrochemistry characterization revealed that decomposition of the triglyme solvent in contact with the charged Si anodes could be voltage-dependent. More basic characterization experiments and electrochemical tests are in progress to explore the degradation mechanism of triglyme and other systems and search for new, stable and passivating electrolyte formulations based on the results.

## References

1.        B. Key, R. Bhattacharyya, M. Morcrette, V. Seznec, J-M. Tarascon, C. P. Grey, J. Am. Chem. Soc., 2009, 131 (26), pp 9239–9249
2.        B. Key, M. Morcrette, J-M. Tarascon, C. P. Grey, J. Am. Chem. Soc., 2011, 133 (3), pp 503–512
3.        Multinuclear Solid-State Nuclear Magnetic Resonance of Inorganic Materials, Volume 6, 1st Edition, Authors: Kenneth MacKenzie M.E. Smith
4.        Q. Zhang, Y. Cui, E. Wang. Modelling Simul. Mater. Sci. Eng. 2013, 21, 074001

# Model Materials Development and Characterization: Lithium Silicate Reactivity

**Jack Vaughey, Baris Key, Binghong Han, Maria Piernas**

Argonne National Laboratory

## Background

The focus of the SEISta program is to develop an in-depth understanding of the underlying reactions, cell environment, and role of sample history that combine to influence the properties of the elemental silicon and the solid electrolyte interphase (SEI).  As the primary protective layer in a lithium-ion energy storage systems, understanding the SEI layer is critical to defining and understanding the various failure mechanisms that can lead to performance degradation.  For silicon-based systems in particular, an understanding of the SEI layer is critical as many of the hypothesized causes of capacity fade and poor Coulombic efficiency are, at their core, derived from an unstable SEI layer.  We have focused on identifying, synthesizing, and characterizing materials that are representative of the silicon/electrolyte interface at various states of charge as a method to gain insight on the formation of the SEI.

## Results

In the recent quarter we focused on extending our understanding of the model compound – binder interactions as it relates to side reactions in the electrochemical cell that contribute to capacity fade.  Specifically we are reporting on mechanistic studies in an effort to understand how the reduced silicides ($Li_7Si_3$), which roughly equates to 300 mV (vs Li) in the Li-Si system, react with common binders. In our previous reports we identified the reaction between PVdF and $Li_7Si_3$ as more extensive than with other common binders (i.e. PAA, LiPAA) and collected various types of data, including FTIR, XRD, MAS-NMR, and Raman spectroscopy, regarding this decomposition reaction.  Initial analysis indicated that backbone appears mostly intact, there was no LiF (^{19}F, ^{7}Li NMR), no significant generation of new crystalline phases (XRD), and the amount of diamagnetic lithium salts increased.  Together, with an analysis of the literature on the reactions between Li/Teflon (1,2), Li/Alkanes (3,4), and a reported DFT study of lithium carbides (4), we have initially proposed a model consistent with our data.  While the Teflon ($-CF_2-CF_2-$) systems tend to react extensively with lithium to make LiF and a polycarbon material, the reactions with alkanes yield materials with highly charged backbones with lithium "counterions" or at higher levels of reduction, materials better described as condensed molecular species (e.g. $Li_8C_3$).  For PVdF ($-CF_2-CH_2-$) systems, limited studies have indicated its stability to lower voltages can be ascribed to the hydride anion formally donating electron density to the fluoride anion, stabilizing the $-CF_2-$ moiety in the system (5).  The reactions do not seem to produce $Li_{12}Si_7$ (or silicon, a possible oxidation product) a poly-carbon, or LiF. Pulling these studies together with our data we believe that using $Li_7Si_3$, we are abstracting hydride anions from the backbone creating a salt like component in the binder.  Studies continue to check for the presence of a gas as a reaction byproduct.  FTIR studies (as well as studies from ORNL on Si electrolyte gassing reactions) have indicated some preliminary evidence for Si-F species.  Future studies will focus on the role of gas generation, identification of any gas produced, and a comparison to more reduced silicides.
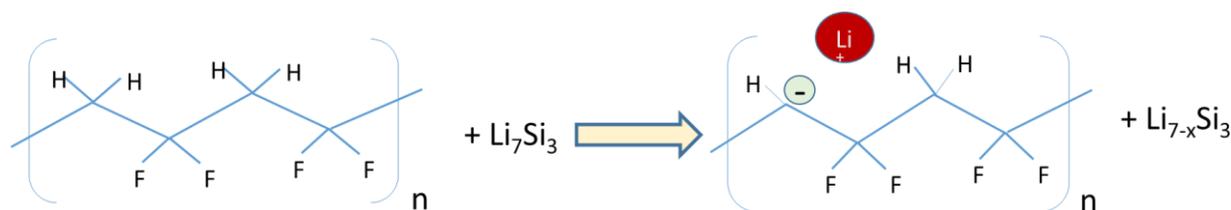
**Figure 1. Proposed reaction between the reduced silicide Li7Si3 and the common binder poly(vinylidene difluoride) (PVdF).**

## Conclusions

Preliminary studies of the reaction between $Li_7Si_3$ (modeling ~300 mV) and PVdF, a common electrode binder, has shown that the polymer is reduced but does not break down to a molecular carbon-containing species. No evidence for a simple lithium salt has been seen although lithium cations appear to have interactions with the polymer backbone. The model is consistent with reported DFT studies and lithium-alkane systems with extra stability induced in the material by the $-CF_2-$ groups.

## References

(1) Nilanjan Chakrabarti, John Jacobus "The Chemical Reduction of Poly(tetrafluoroethylene)" *Macromolecules*, **21**, 3011-3014 (1988)
(2) Osamu Tanaike, Noriko Yoshizawa, Hiroaki Hatori, Yoshio Yamada "Porous Carbons Derived from PTFE Defluorinated with Alkali Metals" *Fuel Chemistry Division Preprints*, **47(2)**, 469 (2002).
(3) Paul v. R. Schleyer "Reexamination of the Structures of Lithium Carbide ($C_2Li_2$ and of $C_4Li_4$)" *J. Phys. Chem.,* **94 (14)**, 5560–5563 (1990).
(4) Yangzheng Lin, Timothy A. Strobel, R. E. Cohen "Structural Diversity in Lithium Carbides" *Physical Review B* **92**, 214106 (2015).
(5) P. Biensan *J.Power Sources,* **81/82** 906 (1999).

## Model Materials Development and Characterization: Prelithiated Si and how it affects the early stage solid electrolyte interphase formation

Yun Xu, Andriy Zakutayev (NREL)

## Background

Early stage SEI formations including electrochemical reduction and chemical reduction were studied in this quarter. SEI can be different due to the electrolyte additive. They can be also formed differently due the reduction pathway, either electrochemically or chemically. In this work prelithiated Si was used to study the chemical reduction of electrolyte and how it's affecting the SEI stability.

## Results

**Electrolyte effect on SEI formation and stability**

1st cycle voltage profiles of lithium silicide in two electrolytes are shown in Figure 1a. Cells were charged first. Not too much difference could be seen from the voltage profiles except the minor differences in OCV. OCV is 0.27V in SE and 0.32V in FEC. Lithiation degree can also be calculated first charge capacity by

$$x = \frac{Q*3600s/h}{Molar(Si)*96500C/mol}.$$

x=1.423 in 200nm Li// 50nm Li. The calculation agrees well with the XPS data with a Li:Si=1:1. Specific capacity was calculated based on the formula calculated from charge capacity. Cycling performance of thin films in two electrolytes are shown in Figure 1a. With FEC，93% of the initial capacity was retained after 100 cycles. But only 30% of capacity was retained with SE. Columbic efficiency with FEC is much stable compared to that with SE. Columbic efficiency and cycling performance difference indicate the electrolyte additive plays an important role in stabilize the SEI and electrolyte. SEM images in Figure 2 show that FEC result in a much smoother surface compared to that without FEC.
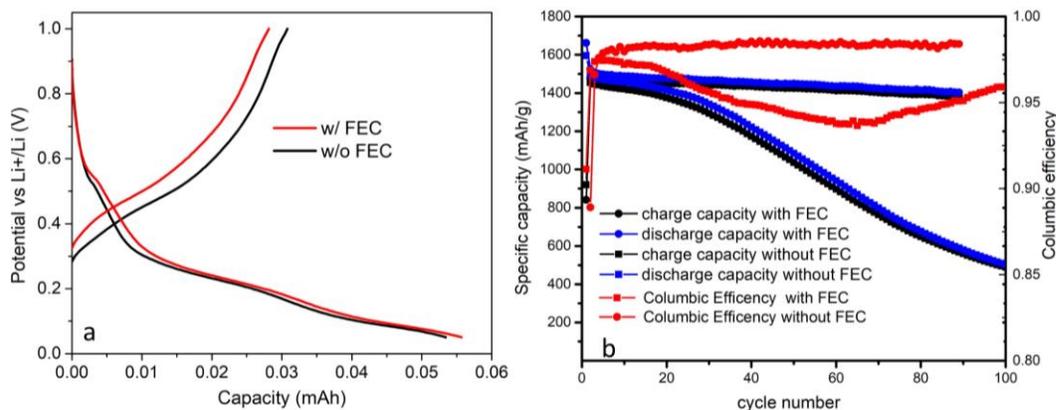


**Figure 1. a) Voltage profiles of lithium silicide cycled in electrolyte with and without FEC; b) Cycle performance in two electrolytes. c) voltage profiles of silicon thin films with and without FEC; d) cycling performance of Si in two electrolytes.**
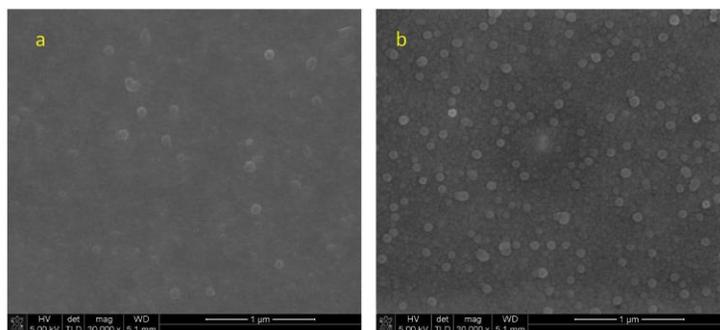


**Figure 2. Lithium silicide thin film surface after exposed to electrolyte. a) with FEC; b) Without FEC.**

**Early stage SEI formation by electrochemical reduction and chemical reduction**

Early stage SEI formation and irreversible capacity can be quantitatively calculated by voltage charge and discharge capacity. Considering there might be a little lithium bound to silicon that's irreversible. This is still a good estimation of how much irreversible capacity due to the formation of SEI. Early stage SEI formation was investigated for both Si and $Li_xSi$ case. Charge and discharge profile of Si in Figure 1a, showed that irreversible capacity comes from the electrochemical reduction at high potential range from OCV to around 0.3V. When Si is prelithiated, we can calculate the lithiation degree by charge the half-cell first. The amount of lithium corresponding to the charge capacity. In figure 1c, cells were discharged first. By calculating how much lithium was originally in the film (from charge capacity in b) and how much lithium was inserted (discharge capacity in c), we can get how much lithium in the film after the 1st discharge. Irreversible capacity due to electrochemical reduction can be calculated by deducting the first charge capacity from the total lithium in the film which is shown in Figure 1d. A very small irreversible capacity was observed in $Li_xSi$ thin film. As previously found in XPS data that there is a pre-formed SEI

on surface Li$_x$Si before electrochemical test. This SEI seems to stop the electrochemical reduction because no irreversible capacity was observed. Prelithiated Si largely eliminate the electrochemical reduction and reduce the irreversible capacity. Cycling performance were collected to see how the early stage SEI formation affect the stability. Figure 2 Shows the cycle performance and columbic efficiency of Si and LixSi. FEC additive was added for both Si and Li$_x$Si. from the columbic efficiency and stability, we note that Li$_x$Si shows a stable performance and more appealing columbic efficiency. Also, we see an increase of columbic efficiency for Si anode, which may be a result from SEI formed from the electrolyte reduction by the freshly exposed lithium silicide. This suggests that early stage SEI formed by electrochemical reduction is not stable as that formed by chemical reduction in Li$_x$Si case.

**Figure 3. a) voltage profiles of Si; b) voltage profiles of LixSi, cell was discharged first; c) voltage profiles of LixSi, cell was charged first; d) irreversible capacity from electrochemical reduction.**


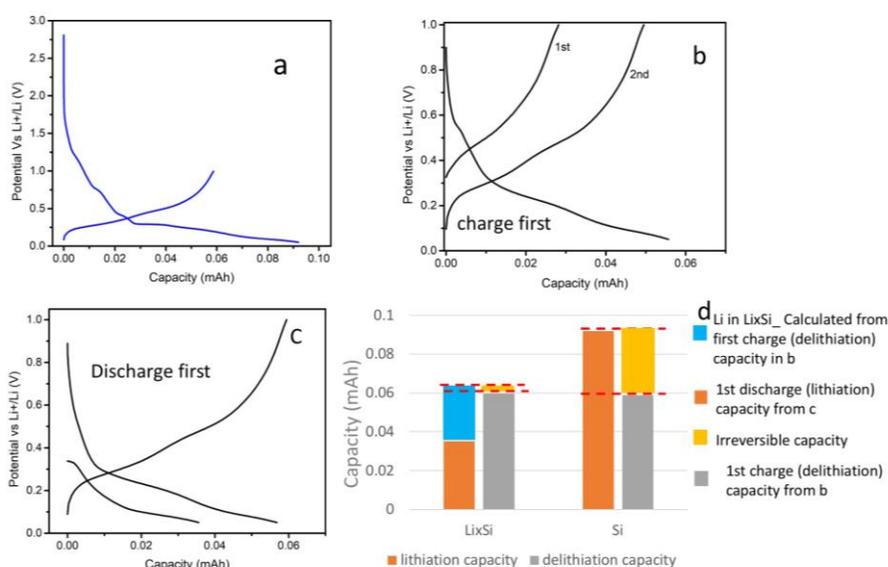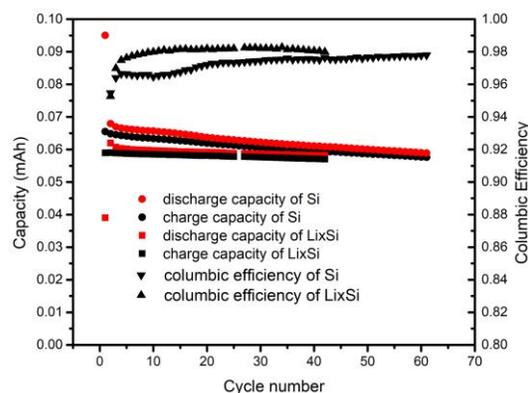
**Figure 3. Cycling performance and columbic efficiency of Si and LixSi.**

## Conclusions

Early stage SEI formed differently due to different electrolyte additives, FEC results in a more stable SEI and stable cycle performance. It is also affected by the surface potential of the electrode. SEI is formed



mainly from the electrochemical reduction on silicon anode. When silicon is prelithiated, SEI is formed

from the chemical reduction; Prelithiation of silicon results in no irreversible capacity from the electrochemical reduction. Prelithiation not only eliminate the electrochemical reduction, but also helps the stability of the electrode and SEI.

## Model Materials Development and Characterization: Fluorescent probes (NREL)  (FY18 Q3)

**Contributors (NREL – Wade Braunecker)**

### Background

In the first two quarters of this year, a Li ion fluorescent probe was developed that could be covalently tethered into binder systems commonly employed with silicon anode materials. Some initial characterization was performed to demonstrate the sensitivity of this probe's absorbance/fluorescence spectra to Li ion concentration. We ultimately aim to develop fluorescent probes that will help determine how components of the silicon SEI layer evolve with cycling. The work specifically contributes to the 3rd quarter SEISta project milestone by complimenting existing strategies to quantify soluble components of the SEI, specifically soluble Li salts. We also envisage the fluorophores will be useful in mapping regions of the electrode that continue to conduct Li well after numerous cycles.

During the recent face-to-face meeting in January, our collaborators helped us identify some challenges and potential pitfalls with this project, including that (depending on the cathode and electrolyte employed) the silicon anode SEI layer can be fluorescent in and of itself.  It was determined that it would be important to have the ability to "tune" the wavelength at which the Li ion probes fluoresce, and significant effort has since been devoted to this aspect of the project. In the second quarter, we reported synthetic progress toward that end. In the third quarter, we finished those syntheses and illustrate here the sensing dynamics of 3 different fluorophores.

### Results

A series of three monomeric fluorophores (M1-M3) were designed with a range of electron donating/withdrawing substituents, whose strength in principle allows the absorbance and emission spectra of these compounds to be tuned so they do not significantly overlap with the background fluorescence of the SEI layer. As can be seen in Figure 1 (top), where the absorbance spectra of each sensor is recorded in the presence of a large excess of Li salt, the "push-pull" effect of the strong electron withdrawing cyano and ester group in the M3 sensor dramatically red-shift the onset of absorbance by nearly 100 nm compared to the electron donating effect of a methyl group (M1). The extended conjugation in M2 results in a very slight red-shift in absorbance relative to M1 by ~10-20 nm. The results indicate excellent tunability of this sensor can be achieved over a range of 100 nm. The bottom half of Figure 1 illustrates that the sensitivity of each fluorophore to increasing concentrations of LiBr are all similar, though the new sensor M3 actually has a slightly increased sensitivity to lower concentrations of LiBr. For example, 0.05 mM of sensors M1 and M2 do not detect the presence of 10 eq. of LiBr (compare blue and purple traces), whereas M3 does begin to respond to this low concentration of Li salt.
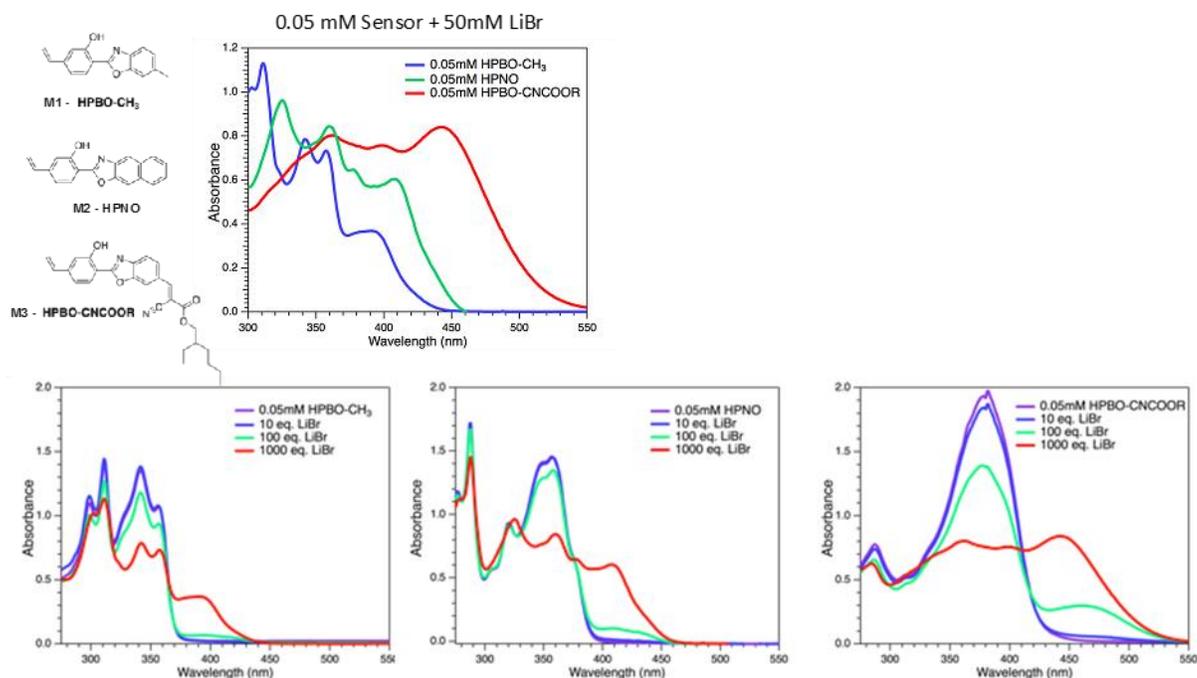
**Figure 1. (top) 3 new monomeric Li ion fluorescent sensors developed in this program with "tunable" absorbance spectra over a range of ~100 nm. (Bottom) Sensitivity of the sensors to various LiBr concentrations.**

## Conclusions

Significant progress was made toward developing Li ion sensors with tunable emission spectra. We have already begun incorporating these binders into actual electrodes for the purpose of imaging their fluorescence with ultra-high resolution techniques through collaboration with LBNL as a first step towards their application to study SEI development.

## Model Materials Development and Characterization: In-Situ Lithiation of Silicon Anode Materials

### Kevin N. Wood, Elisabetta Arca, and Glenn Teeter

## Background

The lack of detailed understanding of the fundamental processes that control lithiation of Si anode materials represents a critical knowledge gap that inhibits the rational design of next-generation batteries. Moreover, the existence of $Li_xSi_yO_z$ phases in the Si-anode SEI is debated within the battery community. Part of the reason for this general lack of knowledge stems from the reactivity of these materials. To help address these issues, NREL researchers are developing a capability to perform XPS measurements during *in-situ* lithiation using a low-energy $Li^+$ ion gun. Developing methods where these reactive materials can be formed and analyzed *in-situ* within an ultra-high vacuum environment chamber will contribute to parallel efforts to interpret XPS and AES data acquired on cycled Si battery electrodes.

In-situ *$Li^+$ ion gun capability provides:*
- *Ability to synthesize baseline $Li_xSi_y$ and $Li_xSi_yO_z$ samples for accurate phase identification*
- *Opportunity to systematically step through the Li-Si-O phase diagram*
- *A method to measure fundamental lithiation processes on specific Si-anode and SEI related phases*

## Results

To investigate the lithiation of $SiO_2/Si(001)$, a 'SEISta round-robin' 50 nm $SiO_2/Si(001)$ sample was subjected to a flux of 10-eV $Li^+$ ions while performing XPS measurements. Current through the sample was ~20 nA, and the $Li^+$ spot size was on the order of 2 mm in diameter. The XPS results during lithiation are shown in Figure 1a. From these data, a clear charging effect can be observed during the initial lithiation, where all peaks shift to higher binding energy by ~7.5 eV, corresponding to a positive increase in the surface electrochemical potential of 7.5 V. This overpotential drops to near zero after about 200 min. of lithiation, likely indicating that the $SiO_2$ layer has been fully converted to one or more $Li_xSi_yO_z$ phases. In the O 1s spectral profile (Figure 1a; green), evolution in the chemical states can be observed between 300-500 min. In that region, the peak initially centered at ~533 eV splits into two peaks around 534.5 eV and 531.5 eV. This might be due to the formation of a more Li-rich $Li_xSi_yO_z$ phase. On the other hand, the data also indicate that $Li_2O$ may be forming during this time. After the XPS *in situ* lithiation measurement, the sample was depth profiled using Auger electron spectroscopy (AES), as shown in Figure 1b. These data clearly show three compositionally distinct regions within the sample, including a $Li_xSi_yO_z$ phase at the surface, a buried $Li_xSi$ layer, and the bulk Si wafer.

In addition to the measurements summarized above for 50-nm $SiO_2/Si(001)$, preliminary *in-situ* lithiation experiments have also been completed on native oxide/Si(001), and on sputter-cleaned Si(001). The XPS data sets comparing evolution of these different surfaces during *in-situ* lithiation are shown in Figure 2. From these data, it is clear that differences in the XPS spectra, corresponding to differences in evolution of various Li-Si-O phases, can be observed depending on the initial condition of the Si wafer. Perhaps the most striking difference is a low binding-energy peak in the Li 1s core level, possibly associated with Li-rich Li-Si phases, that is significantly more intense when less surface oxide is present. To our knowledge, these Li 1s peaks have not yet been described in the literature, and additional studies will be needed to conclusively assign them to particular phases.
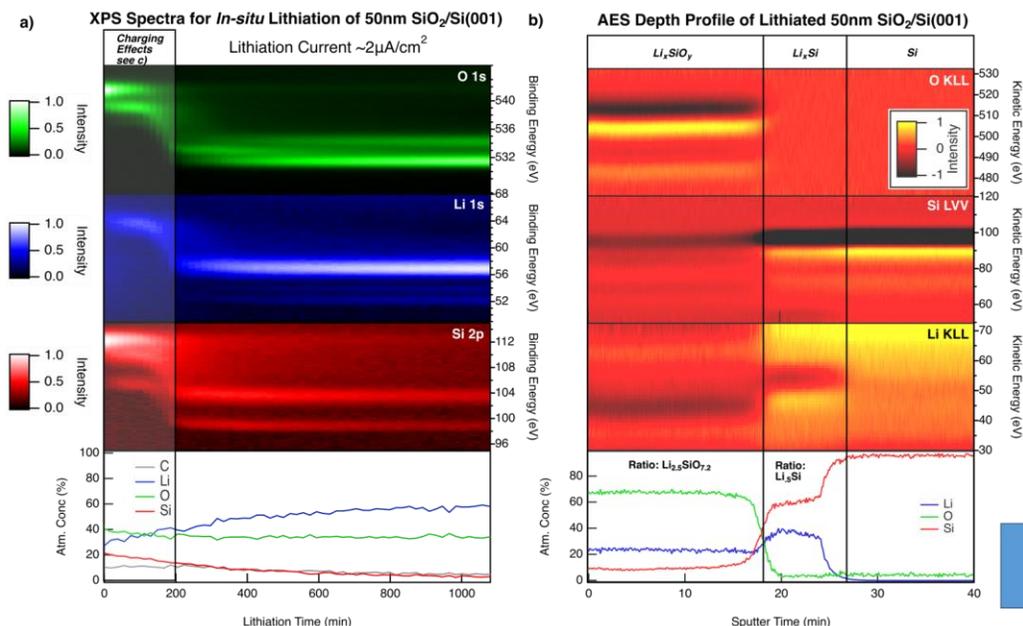


**Figure 1. a) Evolution of XPS core-level spectra during *in-situ* lithiation of 50-nm $SiO_2/Si(001)$ wafer. b) AES depth profile of the lithiated sample reveals that the entire $SiO_2$ layer has been converted to a $Li_xSi_yO_z$ phase; and that an underlying $Li_xSi$ phase has also formed.**
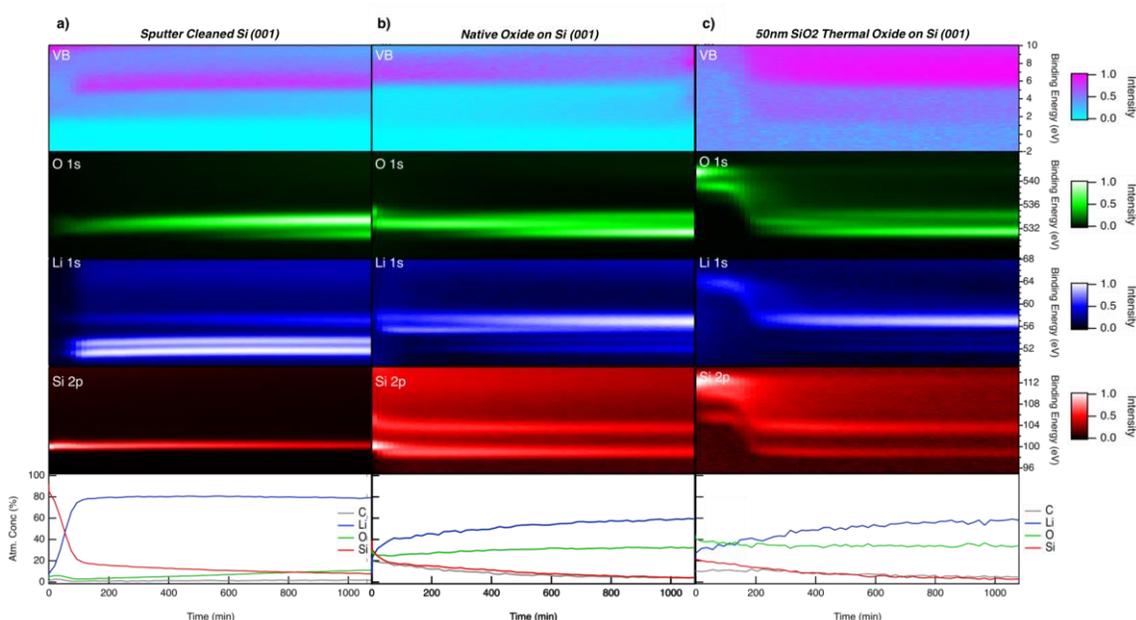
**Figure 2. Evolution of XPS core-level spectra during *in-situ* lithiation of a) a sputter cleaned Si(001) wafer, b) a wafer with a native oxide, and c) an Si (001) wafer with a 50-nm thick thermally grown SiO$_2$ layer.**

Comparing spectra acquired with and without Li$^+$ ion gun current bias enables determination of overpotentials associated with lithiation for the various Si wafer samples that were studied. As can be seen in Figure 3, the overpotential associated with lithiation of the 50 nm SiO$_2$/Si (001) is ~7.5 V. Compared to the native oxide/Si(001) sample, this overpotential is over 100x larger in magnitude, even though the SiO$_2$ layer (estimated ~2 nm for native oxide) is only ~25x thicker. This observation supports the conclusion that excessively thick SiO$_2$ layers will significantly increase cell overpotentials during the first cycle of a Si-based anode.
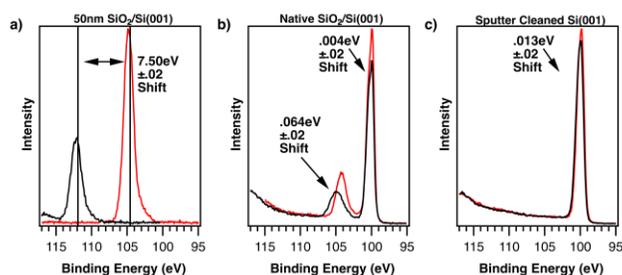


**Figure 3. Overpotential variations for the three different Si wafers tested: a) 50-nm SiO$_2$/Si (001) b) native oxide on Si (001) and c) sputter-cleaned Si (001). The black curve was acquired with the Li+ ion gun current bias on and the red curve without. Binding-energy shifts can be used to estimate overpotentials of lithiation, and ultimately Li diffusivity as a function of Li-Si-O phase.**

## Conclusions

A novel method for studying the fundamental lithiation processes of Si-based anode materials has been demonstrated. Preliminary results show that *in-situ* lithiation via a Li$^+$ ion gun combined with XPS measurements effectively probes the lithiation of Si- based electrodes. These data will help with phase

identification, validation of theoretical Li-Si-O ternary phase diagram predictions, and the quantification of fundamental lithiation properties (e.g., chemically resolved overpotentials, impedances, and Li$^+$ diffusivities).

## SEI Characterization: Understanding and Design of the Si SEI from Coupled Molecular Dynamics – First-principles Calculations (UC Berkeley)

Kristin Persson (UC Berkeley)

### Background

Our examination of the Si anode reactions includes modeling of the solvation structures within the bulk electrolyte and the interface of the electrode. We first investigate candidate reaction pathways by examining the solvation structure of the Li ion and electrolyte molecules at the bulk electrolyte and at the interface. As part of the effort, we will elucidate the solvation structure by comparing the simulation results to experiments.

### Results

FTIR was utilized to probe the solvation structure of the electrolyte of EC or EC with FEC additive. The experimental results were then compared with the previously obtained 6-31++g* level quantum chemical calculation results as well as our previous MD simulation results. Both the calculated and experimental IR spectrum were deciphered by quantitatively assigning the peaks with certain species. The integral area is calculated to obtain the percentage of each species.
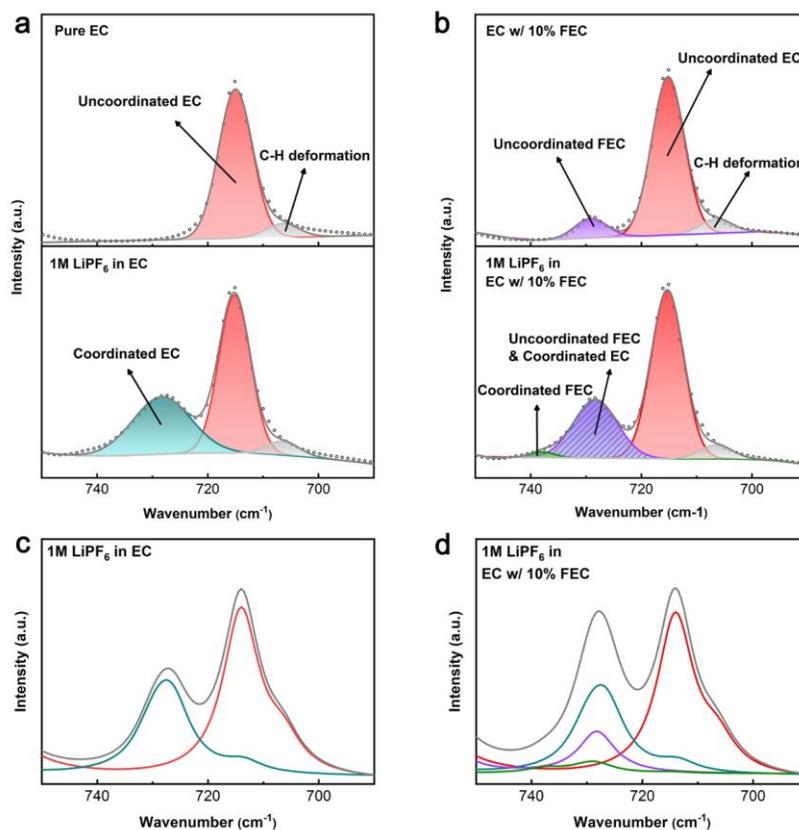


**Figure 1. Experimental FTIR spectra of the C=O breathing mode of (a) pure EC and 1M LiPF$_6$ in EC, and (b) EC with 10% FEC and 1M LiPF$_6$ in EC with 10% FEC. (c-d) The corresponding calculated IR spectra as a comparison of the experimental results.**

The C=O breathing mode was selected as the characteristic vibrational mode. Peaks from experimental results (Figure 1a and 1b) were designated as coordinated ones and uncoordinated ones based on calculation and IR database, which gives us information of solvation structure. The experimental results are in good agreement with the calculated IR spectrum (Figure 1c and 1d), and identical peaks could be found in the spectrum from both methods, in spite that the frequency values have deviations. As for the 1M LiPF$_6$ in EC (Figure 1a,), 38.1% of EC molecules are coordinated with Li$^+$ ion, which corresponds to a coordination number (CN) of 5.13. While the calculated CN (5.84) from MD simulations is slightly higher than the experimental result, both approaches indicated a CN over 5 for the EC electrolyte system. When 10% of FEC additives are included, the free FEC breathing mode would overlap with the coordinated EC vibration mode, which makes it barely possible to obtain the exact percentage of the coordinated and uncoordinated EC. However, it is obvious that the uncoordinated EC area increased compared to the 1M LiPF$_6$ in EC system, which indicated that the CN of EC is lowered. For the other solvent ingredient, FEC, the coordinated number of FEC to Li$^+$ could be directly calculated as 0.21 from the green area, which coincides well with our previous calculation results (0.19) from the MD simulations.
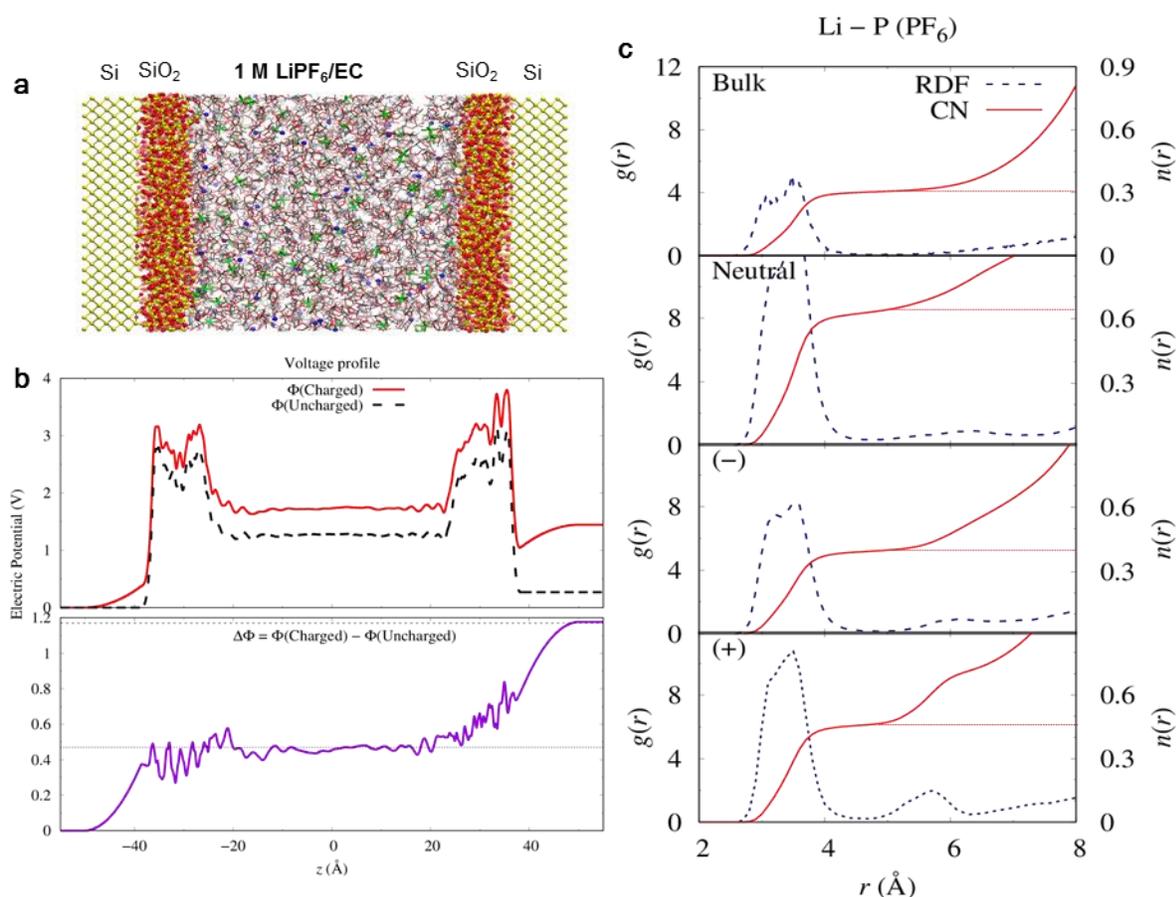


Figure 2. (a) The model of Si anode interface, and (b) the voltage profile in the electrolyte region between the electrodes. The electric potentials are approximately -0.47 V and +0.7 V at the negative and the positive electrodes, respectively. (c) Radial distribution functions and the coordination numbers (CN) of PF6 ions around a Li ion in bulk and at the neutral, negative and positive electrodes, from top to bottom, and the CN values are 0.3, 0.65, 0.4, and 0.45, respectively.

We then analyzed the solvation structure of electrolyte molecules at Si anodes in order to investigate the early stage silicon electrolyte interphase formation on the SEI model. Si anode interface is modeled with amorphous SiO2 layer on top of the crystal silicon electrodes, and equilibrium MD simulation run with 1 M LiPF$_6$ in EC as the electrolyte was produced at 400 K (Figure 2a). Silicon anode under applied voltage is modeled by assigning

a uniform charge, $\pm6.25\times10^{-4}$ $e$ to each silicon atom of negative/positive electrodes so that the voltage applied at the silicon anode is ~ -0.47 V (Figure 2b). The positive Si interface is needed for charge neutrality in the simulation, and the solvation structure is also calculated in comparison to the neutral and negative electrode cases. The coordination number of the Li-$PF_6$ pair, which is assumed to be the CIP ratio, increases from 0.3 to 0.65, in bulk and at the neutral electrode, respectively. Interestingly, the amount of increase in CIP ratio reduces when the lithium ion is at the charged electrodes: with CN 0.4 and 0.45 at the negative and the positive electrodes, respectively. Deeper analysis on the solvation/desolvation at the Si electrode is being conducted.

## Conclusions

1. Based on the experimental and calculated IR spectrum, it is revealed by both methods that the coordination number for EC is over 5. When FEC additive is included, the total coordination number for $Li^+$ would drop, and the FEC would make up a coordination number of ~0.2 in the $Li^+$ first solvation shell.
2. MD simulation result with our silicon anode interface model shows that CIP ratio increases from bulk to $SiO_2$ interface. The neutral silicon interface shows the greatest CIP ratio, and it becomes smaller at the charged interface.

# SEI Characterization: Intrinsic Properties Analysis of 'Individual' Silicon-Electrolyte Interphase Components

Sang-Don Han, Kevin Wood, Caleb Stetson, Elisabetta Arca, Jaclyn Coyle, Yun Xu, Steve Harvey, Glenn Teeter and Andriy Zkutayev (NREL)

## Background

Due to complexity, high reactivity and continuous evolution of a silicon-electrolyte interphase (SiEI), it remains a poorly understood topic in advanced Li-ion battery research, and its detailed and real-time analysis is a great challenge. Thus, one of NREL's tasks characterizes the intrinsic properties of selected 'individual' SiEI components, such as $SiO_2$, $Li_xSiO_y$, $Li_2O$ and LiF, instead of overall complex SiEI. Individual SiEI components are prepared as amorphous thin films, and their chemical composition, homogeneity, morphology and local structure are characterized using a variety of analytical equipment. The physical, electrochemical and mechanical properties of individual SEI constituents, then, are analyzed using electrochemical impedance spectroscopy (EIS), *operando* XPS and SSRM. This study can provide a strong guidance to aid in the development of new electrolytes, additives and binders to stabilize SiEI by identifying beneficial components and providing mechanical explanation of surface chemistry and various reactions/interactions within the SiEI.

## Results

In last quarter LiF and $SiO_2$ were prepared as amorphous thin films, and their homogeneity and chemical composition were confirmed using ToF-SIMS and XPS depth profiling. Their physical and electrochemical properties (e.g., ionic conductivity and activation energy) were characterized using an electrochemical impedance measurement method, and possible phase transition (e.g., growth of large grains) of the LiF film with increasing temperature was observed. To verify this, XRD analysis was performed for as-prepared LiF and annealed LiF (at 523 K). Annealing of the LiF film with thermally induced reordering slightly shifts the (111) reflection peak towards higher angle, which is corresponding to a smaller lattice spacing (Fig. 1). The shift is very likely originated by residual stresses present in the film as shown in previous research.[1] The XRD analysis result can prove phase transitions of LiF with increasing temperature and explain about the different conductivity increasing rates in two temperature regions (468 - 498 K *vs.* 528 - 588 K) in previous studies.
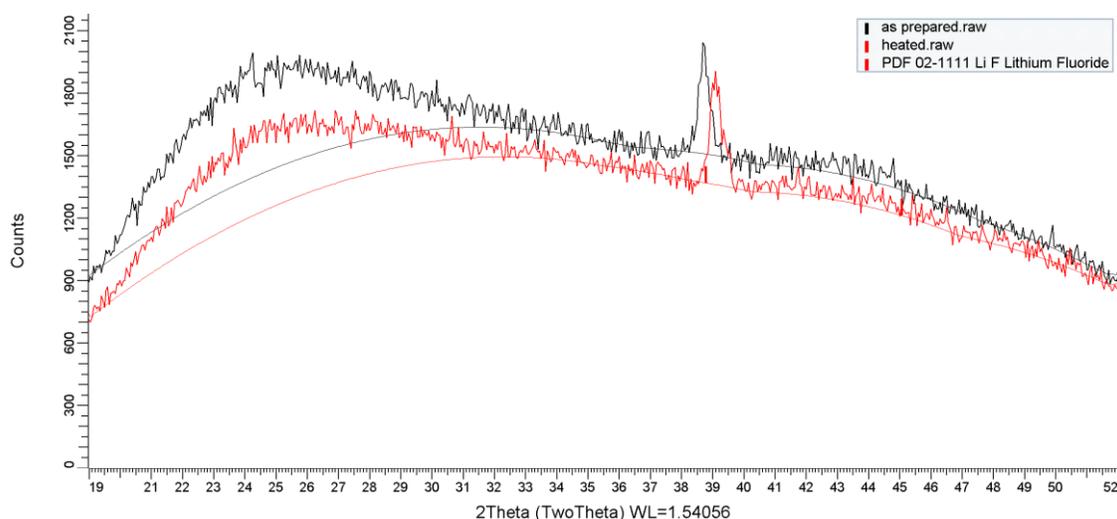
Figure 1. XRD pattern of as-prepared LiF and annealed LiF (at 523K).

The morphology and root mean square (RMS) roughness of the well-prepared LiF and $SiO_2$ samples were analyzed using AFM, while local structure and thickness of them were characterized using scanning spreading resistance microscopy (SSRM) resistivity mapping and depth profiling, respectively. AFM morphology studies showed that Pt-coated Si wafer (as a blank sample for comparison) created a non-trivial amount of surface roughness (2.48 nm RMS roughness). Subsequent deposition of LiF and $SiO_2$ further increased surface roughness (2.77 nm RMS roughness), with $SiO_2$ (3.98 nm RMS roughness) showing higher roughness than LiF. Resistivity mapping at moderate forces at the surfaces of the deposited layers showed very low resistance for Pt-coated Si wafer, and very high resistivity (above the instrumental resolution limit, $10^{10}$ $\Omega \cdot$cm) for LiF and $SiO_2$ (Fig. 2a-c). SSRM depth profiles were carried out to investigate deposition uniformity and thickness. Depositions showed uniformity of electronic properties throughout the deposited layers, and deposited layer thickness was measured at 100 nm (Fig. 2d and e).
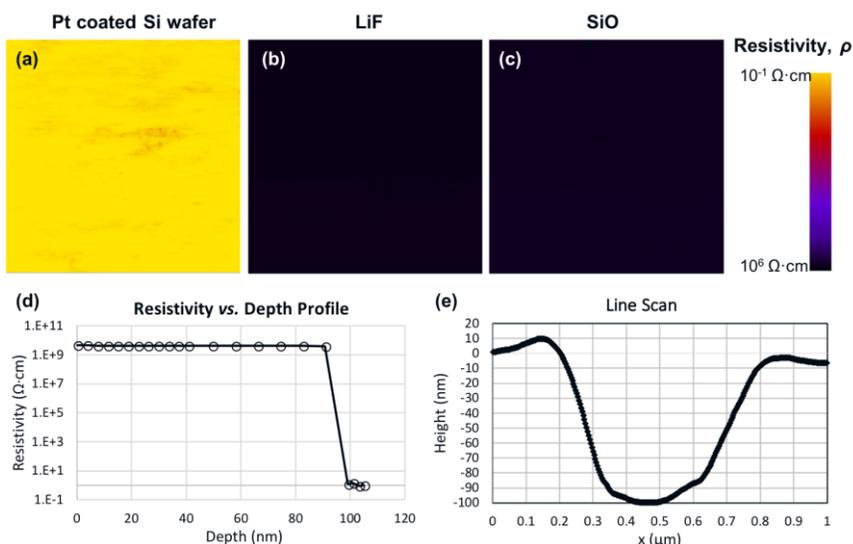


Figure 2. SSRM resistivity mapping of (a) Pt-coated Si wafer, (b) LiF and (c) $SiO_2$. Deposition (d) uniformity and (e) thickness from SSRM analysis.

In addition, nanoindentation was carried out at two determined forces, 15 and 30 µN. At these forces, no indentation was measured on Pt-coated Si wafer, indicating a high measure of hardness. Minor indentation was

measured on $SiO_2$ for these forces (4.5 and 10.5 nm). LiF showed the least hardness, with the two forces resulting in indentation of 11.5 and 36 nm (Fig. 3).

Based on the previous XPS depth profiling results for lithium silicate samples ($Li_xSiO_y$)—segregation of Li at both interfaces possibly due to the lower Gibbs free energy for $Li_2O$ *vs.* $Li_xSiO_y$ and the presents of oxygen at both interfaces—further experiments in this quarter have focused on making the correct stoichiometry of the desired films in order to correctly study their properties. One suggested approach is to prepare the thicker samples as demonstrated in the previous research.[2] We believe the preparation of the samples without segregation of Li at both interfaces is really challenging, so relatively thicker film can alleviate the effect of segregated Li on overall film properties. Thus, $Li_2Si_2O_5$ and $Li_2SiO_3$ were prepared as thicker films (200 nm *vs.* 100 nm in the previous research) to make as close as the correct stoichiometry in the overall samples.
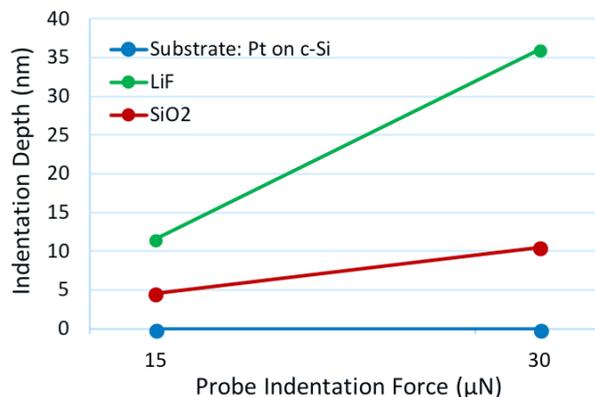


**Figure 3. AFM and SPM (scanning probe microscopy)-based Nanoindentation.**

The XPS depth profiling of the $Li_2SiO_3$ was performed using an $Ar^+$ (beam energy 3keV) sputtering source. The stack layout was $Li_2SiO_3$/Pt/Si (substrate) and the $Li_2SiO_3$ film thickness was around 200 nm. Prior to the measurements, the XPS system has been calibrated to ensure that the measuring spot was aligned to the center of sputtering crater. A first set of measurements (not shown) revealed that the sputtering rate of this material is substantially higher than the sputtering rate measured on a reference sample ($SiO_2(100)$/Si, commercial film) when the standard beam raster parameters are used (3 x 3 mm crater). Therefore, the sputtering crater was increased to a size of 6 x 6 mm and spectra for the core-levels were recorded with a 2 minutes increment. The Fig. 4a reports the atomic percentage of the main three components (Li, Si, O) as well as the substrate on which the films was grown (Pt-coated Si) as a function of sputtering time. The atomic concentrations were determined using the sensitivity factors implemented in the Multiplex program, which are correct to determine the Si:O ratio in sputter-profiling of the reference $SiO_2$ standard. The results acquired on both the 3 x 3 mm and 6 x 6 mm crater show the same trend: the Si:O ratio is roughly constant and homogenous throughout the film, whereas an inhomogeneous distribution of Li is observed. The Li:Si ratio is slightly Li-rich at the surface, while the material appears to be progressively Li-poor/Si-reach throughout the thickness, and enriched in Li again at the interface between $Li_2SiO_3$ and Pt. Additional measurements making use of different sputtering source (e.g., Ar clustering *vs.* standard $Ar^+$) on twin samples would be required to completely rule out the possibility of a measurement artifact caused to the specific sputtering method used in this study. Moreover, use of standards to accurately determine the sensitivity factor for this material would be required for an accurate quantification.
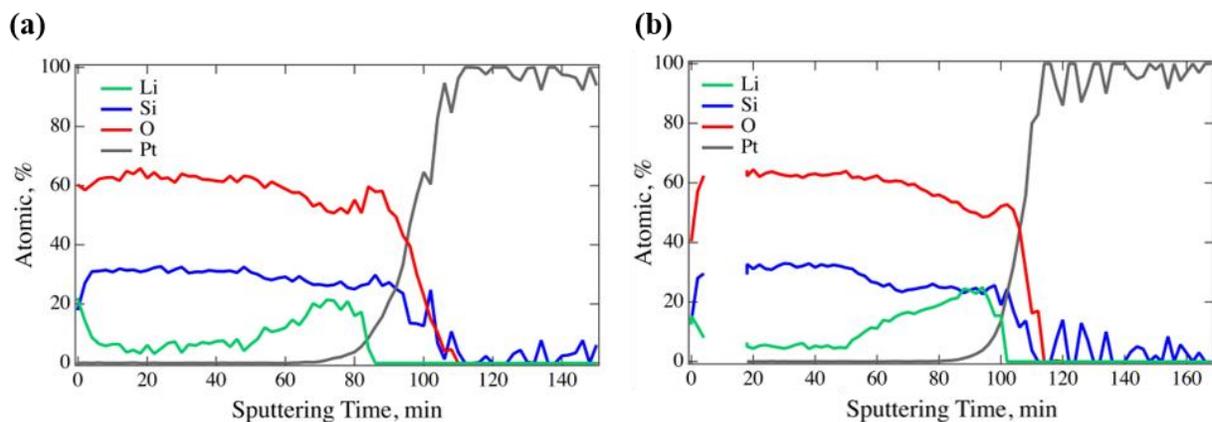
**Figure 4. Comparing sputter deposited films trying to reach a final composition of (a) Li$_2$SiO$_3$ and (b) Li$_2$Si$_2$O$_5$.**

The Li$_2$SiO$_5$ sample (around 200 nm) was analyzed using the same method (Fig. 4b). During the sputtering cycle, the X-ray source turned itself off and thus the missing data-points are due the sputtering interval when data were not acquired. Due to the destructive nature of sputtering process, the measurements could not be repeated. Despite this small glitch, the trend observed for this sample is identical to that observed in the previous sample: both the surface and Li$_2$SiO$_5$/Pt interface appear to be enriched in Li, whereas central region of the films appears to be Li-poor, confirming the need to verify whether or not this problem is due to the homogenous distribution of the elements in the films or if it is due to an artifact caused by the specific sputtering method used in this study.

## Conclusions

The morphology, roughness, local structure and thickness of well-prepared LiF and SiO$_2$ were characterized utilizing AFM and SSRM analysis. In addition, mechanical properties of those samples were analyzed using nanoindentation technique. The properties analysis of well-prepared (homogeneous and correct stoichiometry) LiF shows that it is not a good Li ion conductor. However, it possesses relatively better mechanical property (less hardness), which may be helpful to alleviate pulverization of a Si anode by volume expansion. Overall, it is hard to say whether LiF is a beneficial component within SiEI due to lack of comparing SiEI components. Other individual components of SiEI, lithium silicates (Li$_x$SiO$_y$), were prepared as thicker films (200 nm) to make the samples with correct stoichiometry, but they still show the segregation of Li at both interface. Further experiments are required to completely rule out the possibility of a measurement artifact caused to the specific sputtering method used in this study and to prepare the correct stoichiometry of the desired films in order to correctly study their properties.

## References

1. G. Baldacchini, M. Cremona, S. Martelli, R. M. Montereali and L. C. Scavarda Do Carmo, *Phys. Stat. Sol.* **1995**, *151*, 319.
2. J. Coyle, C. Apblett, M. Brumbach, J. Ohlhausen and C. Stoldt, *J. Vac. Sci. Technol. A* **2017**, *35*, 061509-1.

## SEI Characterization: Early Stage SEI Formation SEISta

Caleb Stetson, Andrew Norman, Chun-Sheng Jiang, Mowafak Al-Jassim (NREL)

## Background

The structural and compositional characteristics of the solid electrolyte interphase (SEI) at early stages of formation are known to be highly dependent on electrolyte chemistry, electrochemical cycling parameters,

and the model silicon system utilized in the battery cell. Investigation in this quarter focuses upon morphological, structural, chemical, and electronic characterization of the SEI formed on differing Si model systems utilizing scanning probe microscopy (SPM) and scanning transmission electron microscopy (STEM).

## Results

Early stage SEIs, formed under highly constrained cycling cutoff voltages (<400 mV, with little to no lithiation/delithiation occurring) on native oxide Si wafers were analyzed with atomic force microscopy (AFM) in tapping mode and scanning spreading resistance microscopy (SSRM) in contact mode. Surface morphology of these SEIs were measured with AFM to establish trends for root mean square (RMS) surface roughness. SSRM was employed to measure total SEI thickness and compare electronic resistivity of superficial regions of SEI. Dozens of samples were characterized to determine the effects of varying cutoff voltage, cell resting, and total number of cycles. Trends for early-stage SEI formation in Gen2 electrolyte can be seen in the table below.

### Table-1: Early-Stage SEI Development

| *Effect of* | Surface Roughness | SEI Thickness | SEI Surface Resistivity |
|---|---|---|---|
| Resting (No rest vs 50 Hours) | Decreased Roughness (3.3 nm → 1.8 nm) | Increased Thickness (2.8 nm → 3.4 nm) | Less Resistive SEI ($10^9\,\Omega\cdot cm \rightarrow 10^6\,\Omega\cdot cm$) |
| Higher Cutoff Voltage (115 mV vs. 400 mV) | Decreased Roughness (8.0 nm → 3.3 nm) | Decreased Thickness (2.8 nm →1.5 nm) | Less Resistive SEI ($10^9\,\Omega\cdot cm \rightarrow 10^5\,\Omega\cdot cm$) |
| Increased Number of Cycles (26 vs 48) | Decreased Roughness (3.3 nm → 1.25 nm) | Increased Thickness (2.8 nm → 3.5 nm) | More Resistive SEI ($10^9\,\Omega\cdot cm \rightarrow 10^{10}\,\Omega\cdot cm$) |

Another study focused on identifying morphological and compositional differences between SEIs formed on two model systems: 15 nm $SiO_2$ dry thermally-grown film on c-Si and a native oxide c-Si. An experiment to investigate stability of the thermally-grown oxide immersed in Gen2 electrolyte for 2 days and 7 days showed that in the absence of electrochemical reactions the oxide film is completely stable in Gen2 electrolyte, and thus the disappearance of the oxide film in the cycled samples results from the electrochemical reaction. An SSRM depth profile of a 15 nm $SiO_2$ on c-Si sample after soaking in Gen2 electrolyte for 7 days can be seen below in Fig. 1, demonstrating the electronic contrast visible between the intact $SiO_2$ layer and the underlying c-Si after mechanically milling down to the interface.
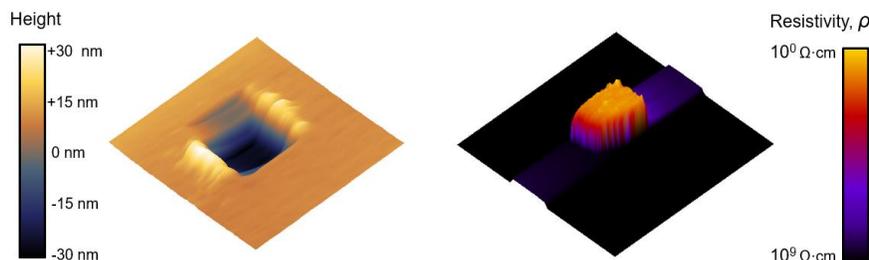


Figure 1. SSRM depth profiling on 15 nm $SiO_2$ on c-Si sample after soaking in Gen2 electrolyte for 7 days. Height image is shown at left, while resistivity image is shown at right. Electronic contrast between $SiO_2$ and c-Si is manifest at a depth of 15 nm, showing that the integrity of the $SiO_2$ film is retained after soaking in Gen2 electrolyte.

SEI from the two model Si systems after 1-2 cycles was studied with SPM and STEM. SSRM resistivity vs. depth profiles showed that after cycling under identical conditions (1 cycle, Gen2 electrolyte, 22 $\mu$A cm$^{-2}$ fixed current density, 5 hours per half cycle), dramatically different SEIs developed on the two systems. On the first sample, 15 nm $SiO_2$ thermally-grown on c-Si, a thin (18 nm), highly resistive SEI developed, whereas on the second sample, native oxide on c-Si, a thicker (50 nm) SEI developed with much lower resistivity throughout. STEM high-angle annular dark-field images and energy-dispersive X-ray spectroscopy (EDS) images captured from the same $SiO_2$ sample and a comparably cycled native oxide sample verified trends for thickness and showed interesting results for chemical composition.
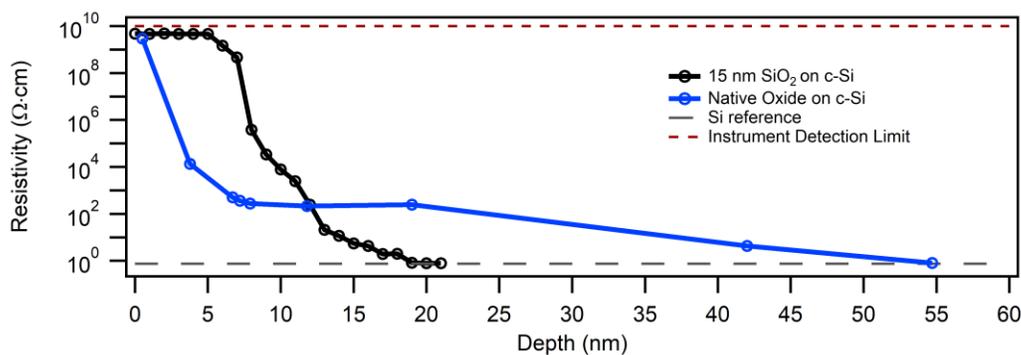


Figure 2. SSRM resistivity vs. depth profiles of SEI formed on 15 nm $SiO_2$ and native oxide on Si wafers after one cycle.
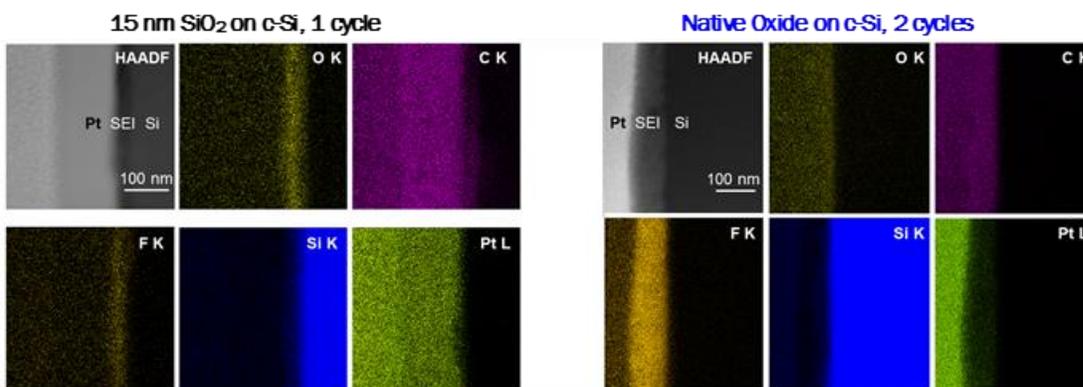


Figure 3. STEM high-angle annular dark-field images and EDS maps of O K$\alpha$, C K$\alpha$, F K$\alpha$, Si K$\alpha$ and Pt L$\alpha$ for two SEIs, the first (left) formed from 1 cycle on 15 nm $SiO_2$ on c-Si and the second formed on native oxide c-Si after two cycles.

EDS maps show that the highly resistive SEI formed from cycling $SiO_2$ on Si have much higher contents of C and O and a much lower F content when compared to the SEI formed on native oxide.

## Conclusions

Early-stage SEI characterized with SPM showed distinct trends with respect to alterations to resting protocol, cutoff voltage limit, and total number of cycles. These trends showed that resting the cell after cycling decreased roughness, increased thickness, and formed a less resistive SEI. Utilizing a higher cutoff voltage limit led to the formation of SEI with decreased roughness, thickness, and less electronic resistivity. Continued cycling served to decrease surface roughness, increase thickness, and increase SEI resistivity.

SEI formed on a thin film of $SiO_2$ on c-Si showed interesting electronic, structural, and chemical properties when compared to that formed on native oxide on c-Si. Electronic resistivity measured via SSRM resistivity vs. depth profiling showed that a thinner, more resistive SEI formed on the $SiO_2$ model system. STEM characterization verified the thickness trend and also indicated a higher composition of C and O and lower levels of F in this SEI. High electronic resistivity may thus be a result of greater relative organic

composition. Moreover, these results suggest that the initial SEI formation mechanism on $SiO_2$ depends on an intermediate $Li_xSiO_y$ phase that forms during lithiation, as the $SiO_2$ film is no longer present after cycling.

## SEI Characterization: In Situ Study of SEI formation

Katie L. Browning (ORNL, UTK), Gao Liu (LBNL), Gabriel M. Veith (ORNL)

### Background

The goal of this project is to better understand the polymeric binder affect on the solid electrolyte interface (SEI) formation and chemistry on Si anodes. To achieve this in situ neutron reflectometry was used. Neutron techniques are more deeply penetrating than x-rays in addition to being sensitive to lighter elements such as a Li and H. From fits to reflectivity patterns the thickness, roughness, and/or diffuseness of the layers can be determined giving a better understanding of buried interfaces. However, the most important parameter learned is the scattering length density (SLD) which gives the composition of the layer. In this work a 10 nm Cu layer was deposited onto a single crystal Si substrate followed by the deposition of an amorphous Si (a-Si) film 50 nm in thickness through magnetron sputtering. The n-type conductive polymer binder, PEFM was deposited via spin coating onto the a-Si film and SEI formation was probed as a function of charge.

### Results

In air measurements were performed to measure the as deposited films before contact with electrolyte. It was determined a ~4 nm film of PEFM was deposited onto a 46 nm a-Si layer. In initial contact with the electrolyte (1.2 M $LiPF_6$ in d-EC/d-DMC 3:7) a ~4 nm reaction layer formed on the surface of the anode with an SLD of $3.01 \times 10^{-6}$ $A^{-2}$. Due to the lower SLD value than that of the electrolyte (5.5) it would indicate a Li-rich layer due to H and Li being low coherent scatters therefore lowering the overall SLD, and because deuterated solvents are used there is no H source indicating the layer is rich in Li.

At 1.2 V the polymer doubled in size and takes up around 26% volume fraction within the layer. At this potential the reaction layer has thickened with an increase in the SLD indicating the layer is becoming more organic in nature. At 0.8 V the reaction layer now becomes the SEI as the EC has started to decompose. The SEI layer remained around 5 nm from the previous potential but increased in SLD indicating the decomposition of the electrolyte and organic species forming causing the SLD value to increase as a result of the deuterium. The polymer layer SLD has increased significantly from 2.57 to 5.14 most likely a result of further electrolyte incorporation within the layer. However, because of the increased SLD values at this potential a contrast issue occurs at 0.4 and 0.15 V due to the SEI and polymer layer SLD becoming close to that of the electrolyte. What is determined is a thick diffuse layer forms on the surface of the Si. The lithiation of the Si layer begins at 0.4 V as evidenced by a thickness increase in the Si layer in addition to a lower SLD. At 0.05 V the anode has lithiated to around $Li_{0.7}Si$ and a distinct lithium rich layer has formed on the surface of the anode as evidenced by a lower SLD value and thins to around 7 nm.
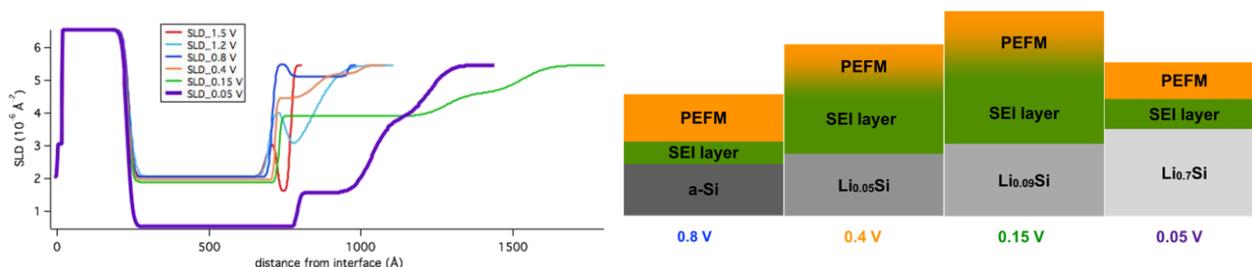
## Conclusions

Upon further cycling of the cell the PEFM layer tends to thicken with lithiation and thin during delithiation. The SEI layer does not exhibit a clear trend after 3 cycles; however, analysis is still on going. XPS samples have been collected following the same cycling procedure for the reflectivity experiment and are being analyzed to further understand the composition of the SEI as a result of the PEFM.

# SEI Characterization: Interaction of LixSiOy with Gen-2 Electrolytes

Jaclyn Coyle (UC Boulder), Kevin Zavadil (SNL), Chris Apblett (SNL)

## Background

This quarter, we have focused on exposure of electrolytes to the model silicates and understanding how the evolution of the SEI is affected by the presence of the silicates, both in time and in composition, after exposure to the Gen 2 electrolyte (without FEC) and the resulting surfaces analyzed using various techniques, including XPS, IR, FIB/SEM and EIS. This supports the Q2 Milestone of "Completed characterization (electrochemistry, IR and Raman) of the early stage silicon electrolyte interphase formation on the SEISta model research samples, specifically by establishing and demonstrating a procedure for quantitatively measuring the solubility of SEI on silicon surfaces".

## Results

### LixSiyO studies

Standard samples of thin film Si (50nm Si/500nm Cu/650um C-Si degenerate/100nm Ti/500nm Au) were prepared and diced using the methods previously described. These samples were then used as substrates for the sputter deposition of 40nm thick lithium silicates of varying compositions ($SiO_2$, $Li_2Si_2O_5$, $Li_2SiO_3$, and $Li_4SiO_4$) expected from the tie line on the Li-Si-O ternary for lithiation of $SiO_2$. These correspond to a 0, 1:1, 2:1, and 4:1 composition of Li:Si. Samples were then exposed to the gen-2 electrolyte (EC:DMC 3:7 1.2M $LiPF_6$) without FEC for varying lengths of time between 30 minutes and 3 days. Earlier experiments in this area were confounded by contamination of F and C from the sputtering process that made quantitative evaluation of the impact of the electrolyte difficult; those issues have been resolved and clean measurements, including both open circuit and cycling, have been performed.
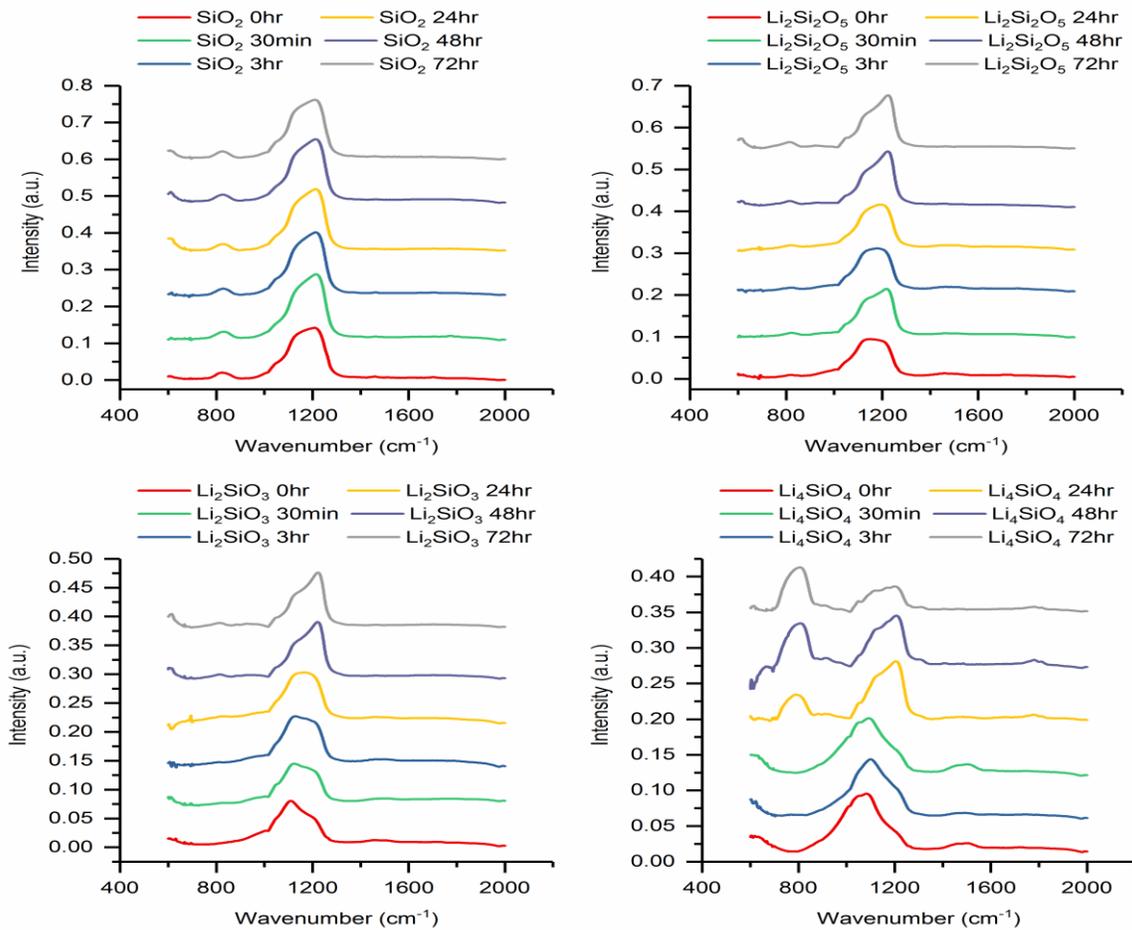
Figure 1: ATRIR data from 50nm Si substrates sputter coated with 50nm silicates of varying composition. Onset of peak shifts to higher wavenumber, indicating a possible disruption of the Si-O-Si network over time. As lithium is incorporated into the matrix, this process accelerates, and by 4:1 Li:Si, the appearance of a new Li alkyl carbonate peak appears, possibly created by accelerated breakdown of the electrolyte due to high Li content in the film.

Data from ATRIR analysis of the samples exposed to electrolyte for times up to 3 days are shown in Figure 1. This data shows that, with increasing lithium content in the silicate, the normally stable $SiO_2$ structure is increasingly subject to changes in structure upon exposure to electrolyte. In $SiO_2$, the Si-O peak at 1200 cm-1 is largely invariate across the exposure time. In the 1:1 Li:Si sample, a distinct shift in peak to higher wavenumbers, possibly indicating disruption of the Si-O matrix, is observed, and this trend is continued in the 2:1 Li:Si samples, with the onset of peak shift occurring earlier. In the 4:1 Li:Si, the peak shift occurs within the first 24 hours of exposure, and a new peak, tentatively identified as Li alkyl carbonate, is observed to grow on the substrate, indicating that the increased Li in the film may be accelerating the decomposition of the electrolyte and leading to the formation of the alkyl carbonates.

XPS data on similarly prepared samples shows a similar story, and is shown in Figure 2. These are depth profile XPS measurements, , but for all of them, the profile is approximately the depth of the silicate (~40nm), with no underlying Si in the depth profiles. In the case of $SiO_2$ (the upper set of data), time evolution of exposure essentially shows no appreciable change in the profiles, with only a small amount of fluorine and carbon coming into the film after the full soaking time. Lithium content in the film is also stable, to the limits of detectability of the Li in the XPS system is constant at around 5-10%. Recall, this film had no Li to begin with, so this Li must be penetrating from the electrolyte.

Contrast this with the Li4SiO4 data (lower set of data), which shows similar starting conditions (with the exception of more Li in the film), but rapid changes in profiles on exposure. Surface levels of fluorine increase dramatically after only 3 hours of exposure to electrolyte, and become significant, all the way through the film, after several days of exposure. The relative Li concentrations, oxygen concentrations, and Si concentrations are also being significantly modified through the depth of the film, possibly through the dissolution of the existing film and recreation of the SEI.
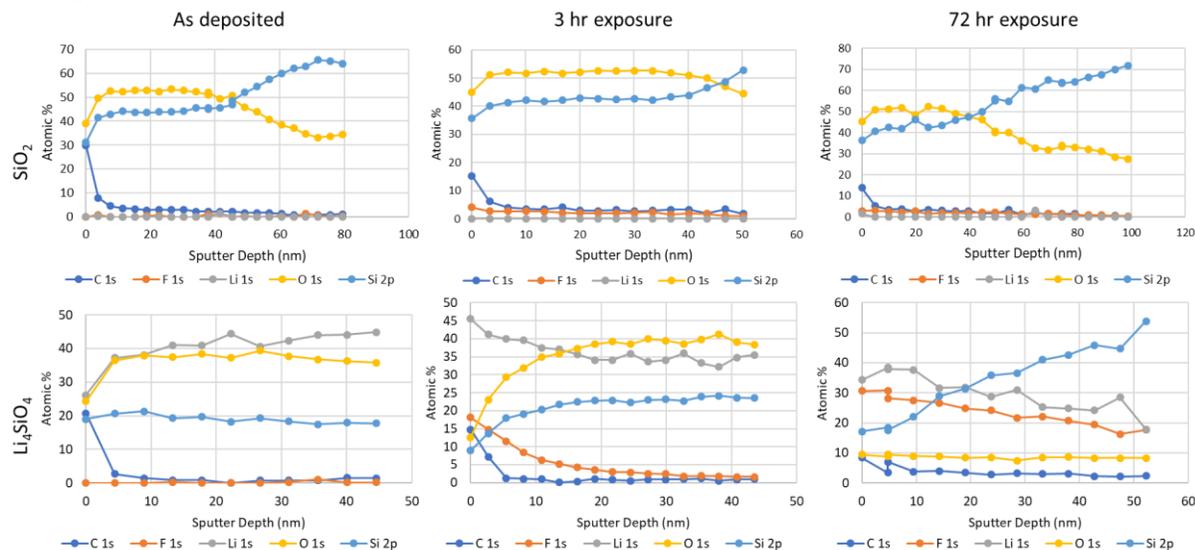


**Figure 2: Depth profile XPS data for SiO2 (top) and Li4SiO4 (bottom) coated samples as deposited (left), after 3 hours of electrolyte exposure (middle) and after 3 days of exposure (right). The existing of Li starting in the silicate dramatically affects how quickly the films change composition, and the admission of fluorine into the films, along with redistribution of oxygen, Li, and Si.**

## *Cell Level Testing*

Electrochemical impedance was started in this quarter, and data for the exposure to electrolyte as a function of composition, time, and temperature is being collected. The initial look, just at room temperature and just for $SiO_2$, is reported here. For this data, the raw impedance curves were modelled as variant of the modified Randles Cell, with no Warburg element (because the films are a flat plate, rather than a diffusion limited powder bed), and an extra capacitance to account for bulk capacitance in the cell.

These models fit the Nyquist plots reasonably well, and allow for interfacial data (charge transfer resistance and double layer capacitance) to be extracted over the time range of the experiment. The bulk values over time do not change within measurement error, but there is an initial slow change in the interfacial resistance and the double layer capacitance. However, a rather abrupt change is observed after several days of exposure, with the interfacial resistance dropping by half, and double layer capacitance increasing by 50% in a matter of hours.
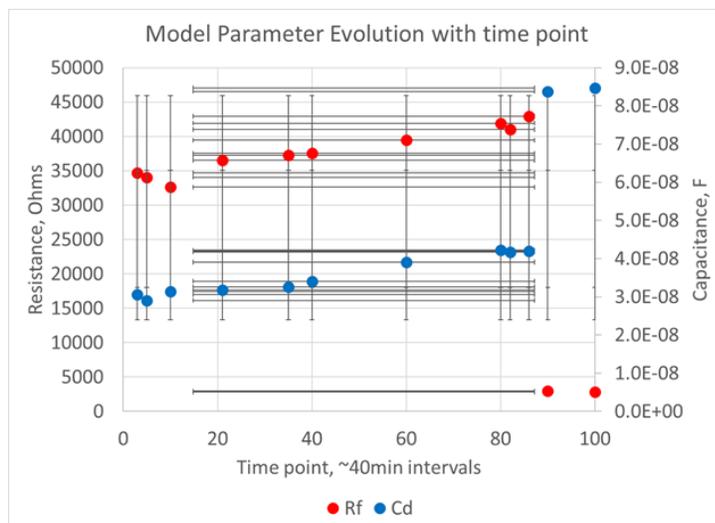
**Figure 3: Double layer capacitance (blue) and interfacial resistance (red) as measured through EIS modelled with a modified Randles circuit on SiO2 at room temperature. Time points are at ~40minute intervals. An abrupt change in these parameters is observed after several days of exposure.**

The reduced data is shown in Figure 3. At present, we do not fully understand this abrupt change, but the experiments as a function of temperature and composition should help in understanding this effect.

## Conclusions

The composition of the starting film, particularly with regard to the silicate composition, has a dramatic effect on the evolution of the SEI as the electrolyte is exposed to the silicon substrate. Both ATRIR and XPS data show that film composition in the absence of lithium (ie, SiO2) is much more stable to electrolyte change than when there is lithium present in the film. In addition, significant fluorine penetration into the SEI is observed when Li has penetrated (or has been deposited) in the film, and a large redistribution of Li, Si, and O occurs as the film evolves over time. Finally, impedance data that is continuously taken indicates that a relatively large shift in electrical behavior is observed after an incubation time of days at room temperature on $SiO_2$, indicating that these chemical shifts may also come after an initial incubation time of slow change in film composition, followed by a relatively rapid degradation or restructuring of the SEI. This may begin to shed light on the issue of shelf life degradation, as slow processes may have to work for a period of time prior to manifesting as a permanent loss of capacity for the system.

## SEI Characterization: Early Stage Formation of the SEI on Silicon wafers (NREL)- FY18, Q3

Yanli Yin, Taeho Yoon, Chunmei Ban (PI), NREL, Golden, CO

## Background

The objective of this project is to develop a systematic understanding of solid electrolyte interphases (SEI) for silicon (Si) electrode materials, and provide practical strategies for stabilization of the SEI in Si-based electrodes. The SEI layer begins to form as soon as the Si electrode contacts the electrolyte. The SEI is comprised of the products from many reduction reactions of salts, solvents and electrolyte additives. These reduction

reaction competes with each other; and the kinetics is heavily dependent on current density, overpotential and the catalytic properties of the electrode surface, finally determine the composition and structure of a SEI layer. Moreover, the phase transformation and mechanical deformation caused by the lithiation/delithiation process present new challenges in investigating the SEI layer. The continuous reduction of electrolyte observed in Si-based composite electrodes may be attributed to the unceasing appearance of new surface during the volume changes, which can obfuscate the study of the interaction between the electrolyte and the Si surface. In order to decouple the interfacial chemistry from the interference of the phase transformation and mechanical deformation, here, we aim to investigate the early-stage SEI (es-SEI) chemistry before the Si lithiation process. This approach enables the study of the sole impact of electrochemical conditions on the composition, structure and chemiophysical properties of SEI. Furthermore, the information collected from the early-stage SEI could provide the new strategies to stabilize the Si electrode surface.

## Results

The intrinsically high sensitivity of SEI to the reaction environment and the surface structure and morphology has contributed to the measurement discrepancies, which causes significant difficulty in fully understanding the chemistry of SEI. Therefore, we have firstly established standard model Si electrodes, cleaning protocols, and cell fabrication procedures to elucidate the convoluted mechanisms of SEI on Si-based electrodes, which has been reported previously.

Si model samples (denoted as SN) established in FY17 have been used in this study. All of the Silicon (Si) electrodes (½ inch x ½ inch) were cleaned with our established multi-step cleaning protocol to remove the surface grease, particles and organic residue. After cleaning, the electrodes were dried in vacuum oven at 100 °C prior to the cell fabrication. The electrolytes selected for this research are 1.2 mol/L $LiPF_6$ (abbreviation "G2" used in the plots) dissolved in the solution comprised of ethylene carbonate (EC): ethyl methyl carbonate (EMC) with the weight ratio of 3:7, respectively. All of the Si electrodes were used as work electrodes in the customized electrochemical cells, where the lithium metal was used as a counter electrode. 7 µl of the electrolyte was used in every cell; and the Celgard 2325 was used as a separator for the cell assembly.

A representative voltage profile of this Si electrode is shown in Figure 1a. The Si electrode was reduced with a galvanostatic reduction current of 6.82 µA cm$^{-2}$ and kept it for the time up to 2 hours. The reduction of electrolyte starts at the beginning of the cathodic process, while the low voltage plateau section of this voltage profile is corresponded to lithiation process and the formation of the amorphous Si. Figure 1a well agrees with the initial lithiation behavior of crystalline Si. Figure 1b shows the differential capacity profile of this Si anode. The two peaks appear at the potential of around 0.250 V and 0.550 V. The deep drop of this differential capacity profile at the potential of 0.060 V indicates the starting of Si lithiation. To quantitatively study the reduction behavior of electrolyte and the Si anode, this differential capacity profile is divided to the following three regimes by the voltage range : Regime 1: a range from the open circuit potential (OCP) to 0.400 V which is corresponded to the reduction behavior around the peak at 0.550 V; Regime 2: a range from 0.400 V to 0.115 V, which is corresponded to the reduction behavior around the peak at 0.250 V; Regime 3: a range from to 0.115 V to 0.060 V, which is corresponded to the inital part of Si lithiation.
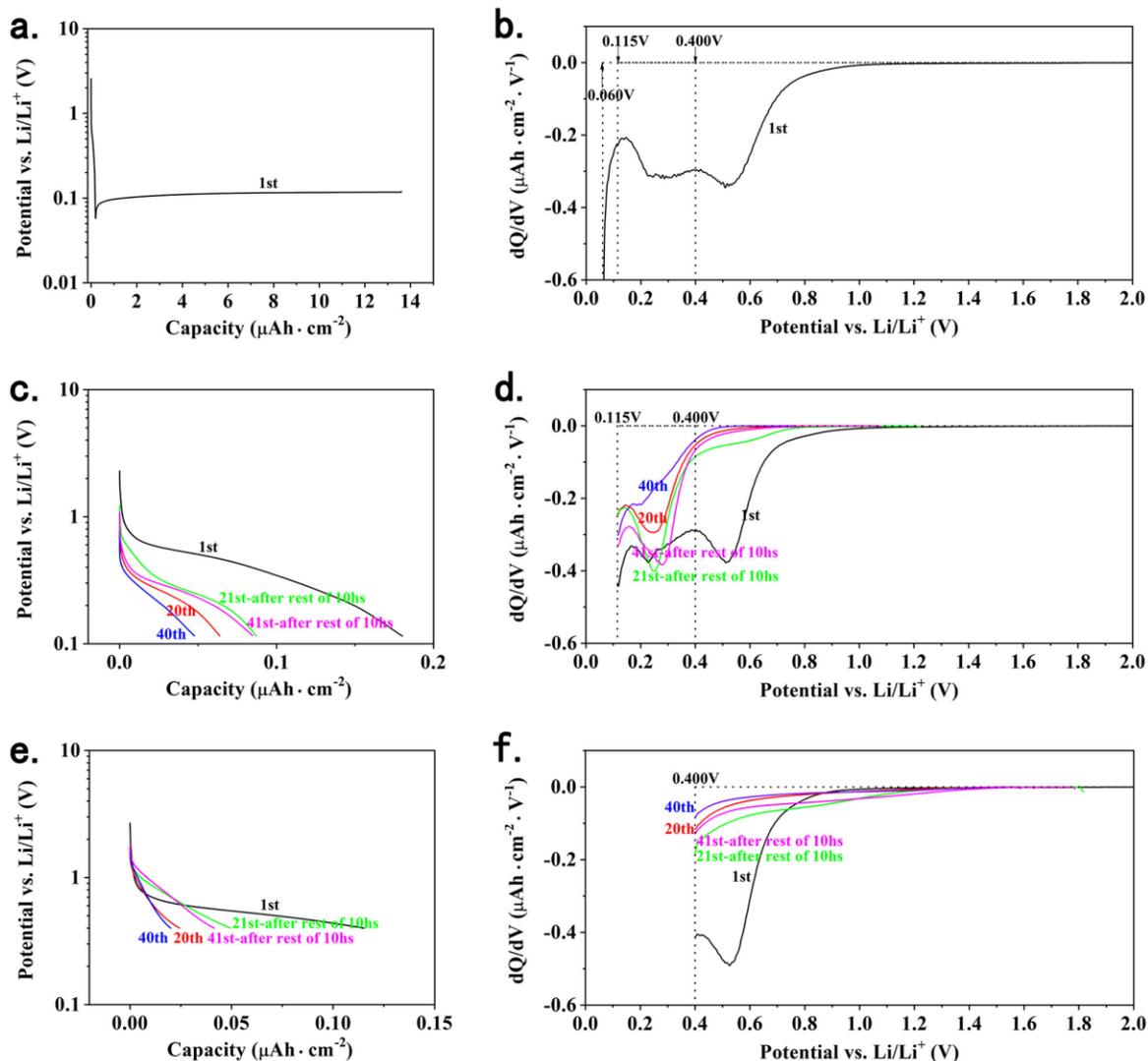
**Figure 1. (a)** The voltage profile and **(b)** the differential capacity profile under the condition including both es-SEI formation and the Si lithiation. **(c)** The voltage profile and **(d)** the differential capacity profile under the HVIST condition of es-SEI formation including regime 1 and regime 2 with the cut off voltage at 0.115 V. **(e)** The voltage profile and **(f)** the differential capacity profile under the HVIST condition of es-SEI formation including only regime 2 with the cut off voltage at 0.400 V.

To decouple the Si lithiation from the electrolyte reduction in the above condition, we designed a unique electrochemical protocol entitled "high-voltage interface stabilizing testing" (HVIST) with the following two procedures. Procedure a including the aforementioned Regime 1 and Regime 2: (1) Apply a galvanostatic reduction current of 6.82 μA cm$^{-2}$ to the cut-off voltage of 0.115 V, then rest for 3 hours, repeat for 20 cycles. (2) Rest for 10 hours, (3) Repeat the setp 1 and step 2 for 10 cycles. Procedure b including only Regime 1: (1) Apply a galvanostatic reduction current of 6.82 μA cm$^{-2}$ to the cut-off voltage of 0.400 V, then rest for 1 hour, repeat for 20 cycles. (2) Rest for 3 hours and 20minites. (3) Repeat the setp 1 and step 2 for 10 cycles.

Figure 1c shows the voltage profile of the Si electrodes, under the HVIST procedure a—with a cut-off voltage of 0.115 V including Regime 1 and Regime 2. Figure 1d shows the differential capacity profile under this HVIST procedure a. Figure 1e shows the voltage profile under the HVIST procedure b—with a cut-off voltage of 0.400 V only including Regime 1. Figure 1f shows the differential capacity profile under the HVIST procedure b. Both Figure 1c and Figure 1e have a slope curve associated to the electrolyte reduction. The plateau curves—responded to lithiation reaction—are missing in both Figure 1c and Figure 1e, because the Regime 3 is

not involved in HVIST procedure a and b. Two peaks can be easily identified in Figure 1d, located at the voltage of 0.250 V and 0.550 V. As expected, only one peak is shown in Figure 1f, at the voltage of 0.550 V. For both Figure 1d and Figure 1f, the intensity of the peak at the voltage of 0.550 V become decreasing after the 1st cycle.
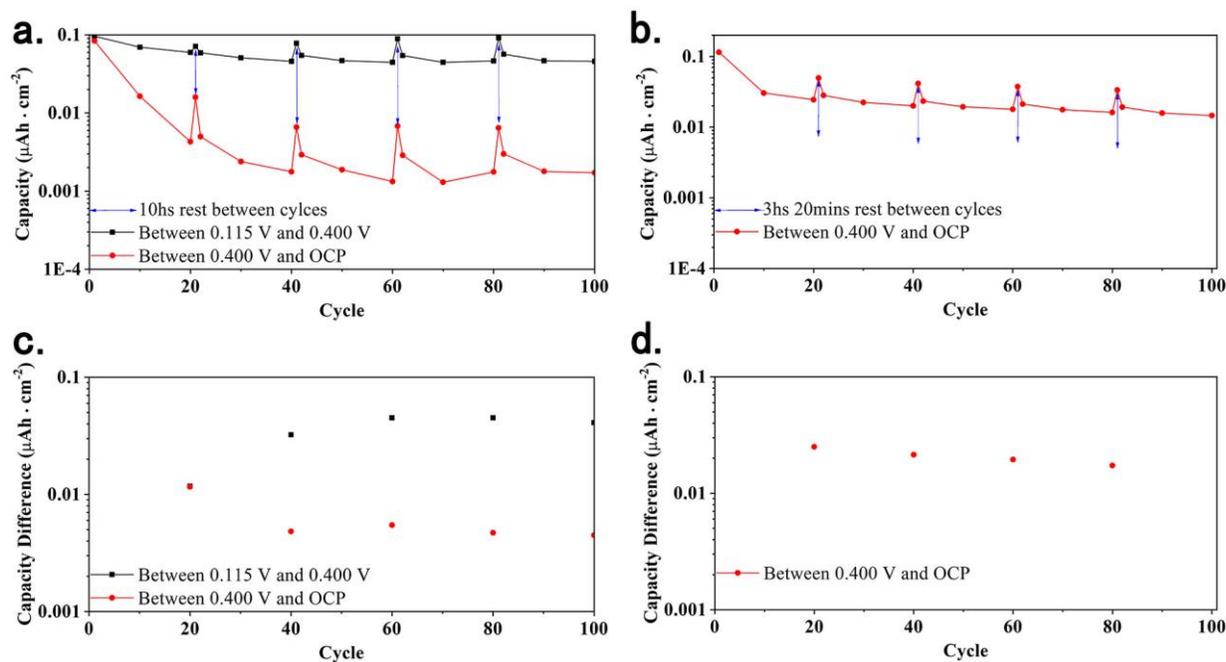


**Figure 2. (a)** The capacity as a function of cycle number for the Si electrode with a cut-off voltage of 0.115V, the plots include the capacity for both Regime 1 (between 0.400 V and OCP) and Regime 2 (between 0.115 V and 0.400 V). **(b)** The capacity as a function of cycle number for the Si electrode with a cut-off voltage of 0.400 V, thereby the capacity is only included Regime 1. **(c)** The capacity difference of Regime 1 and 2, before and after 10hr rest, for the Si electrode with a cut-off voltage of 0.115V, **(d)** The capacity difference of regime 1 before and after 10hr rest, for the Si electrode with a cut-off voltage of 0.400V,.

In order to quantitatively monitor the evolution of the reduction activities, the change of capacity in each regime as a function of cycle number is plotted in Figure 2. Figure 2a shows the capacity as a function of cycle number for the Si electrode with a cut-off voltage of 0.115V, thereby, the capacity plots include both Regime 1 (between 0.400 V and OCP) and Regime 2 (between 0.115 V and 0.400 V). Figure 2c shows the capacity difference before and after long rest for the Si electrode with a cut-off voltage of 0.115V. Figure 2b shows the capacity as a function of cycle number for the Si electrode with a cut-off voltage of 0.115V, therefore, the plot only includes the capacity difference in Regime 1. Figure 2d shows the capacity difference before and after long rest, for the Si electrode with a cut-off voltage of 0.115V. As indicated in both Figure 2a and 2b, the capacity for both Regime 1 and 2 is continuously decreasing with the cycle number, depicting that the reaction activities are gradually reducing during the repeated galvanostatic reduction process. However, the Si electrodes cannot be passivated with the es-SEI within 100 cycles. Interestingly, capacity difference is observed after 10 hr resting for both Regime 1 and 2, which indicates that some reduction reactions re-occur after the rest.

## Conclusions

The research in this quarter demonstrates the electrochemical behavior when using different cathodic conditions. In order to better understand the early-stage SEI chemistry, a new methodology has been developed here to decouple the lithiation-induced mechanical deformation and phase transformation from the SEI formation, to directly investigate the interphase formation and evolution. Galvanostatic reduction was performed on the Si anode with a specific cut off voltage before Si lithiation voltage, which allows the formation of an early-stage

SEI without the involvement of phase transformation and mechanical deformation. The special cut-off voltage is set for the galvanostatic reduction process of the Si anode. The formation of early stage SEI is continuously in these repeated cathodic process. The reduction reactions re-ocurred after a 10-hour resting, which may indicate the deattachment of the early stage SEI during the rest. The detachment and reoccurance of the early stage SEI could cause the low coulumbic efficiency and non-passivation behavior of the Si electrodes. Further investigation has been planned by using surface analysis and characterizing techniques, will be reported in next quarterly reports.

## SEI Characterization: Spectroelectrochemistry on Silicon Oxide Coated Silicon Wafers. [LBNL]

Ivana Hasa, Atetegeb M. Haregewoin, Liang Zhang, Jinghua Guo, Philip N. Ross and Robert Kostecki

### Background

The primary objective of our effort is to clarify and understand the processes occurring at the silicon/electrolyte interface. The reductive decomposition of the electrolyte in lithium-ion systems employing silicon anodes is inevitable, since the working potential of the electrode is far below the electrochemical stability window of the electrolyte components. In principle, the insoluble decomposition products precipitating on the electrode surface, result into the formation of a passivating surface film which suppress further electrolyte decomposition.[1,2] However, the inherent instability of the silicon/electrolyte interface strongly inhibits the surface passivation, which is further endangered by the mechanical instability of the electrodes, which upon alloying with lithium experience a huge volume expansion responsible of active material cracking and consequent instability of the passivating film.[3] A better understanding of the kinetic processes occurring upon cycling will enable an efficient implementation of silicon based electrodes in high performance lithium-ion batteries. To accomplish this we address the inherent non-passivating behavior of silicon model electrodes in organic electrolytes.

In order to de-couple the processes caused by the volume expansion and the inherent non passivating behavior of silicon, the model electrodes of choice are represented by sputtered silicon thin film deposited on copper current collector, which represent the SEISta model research samples.

The model electrodes, fabricated at ORNL, are constituted by 50 nm silicon thin film with a 3 nm native oxide and a grown 10 nm $SiO_2$ surface layer.

Our effort in the last quarter has been mainly focused on the investigation of the interfacial properties of the silicon thin film electrodes and the characterization of the surface chemistry and composition upon cycling, including the nature of the electrolyte decomposition products and the effect of the silicon oxide on the interfacial properties. A complete comparative characterization, in terms of electrochemistry and ATR-FTIR analysis has been performed to investigate the SEI and understand its stability.

### Results

The electrochemical processes occurring at the silicon thin film/electrolyte interface have been investigated through ex-situ ATR-FTIR analysis. Two types of SEISta model thin film electrodes, i.e. 50 nm Si + 3 nm $SiO_2$ and 50 nm Si +10nm $SiO_2$ have been cycled at a constant current of 5 μA cm$^{-2}$ within the 0.05 V- 1.5 V vs Li$^+$/Li potential range using 1.2M $LiPF_6$ in EC:EMC 3:7 wt.% as electrolyte solution. The cells have been stopped at different state of charge and the electrodes have been recovered for ex-situ analysis. To avoid any alteration of the electrode's surface, the ATR-FTIR investigation has been performed under inert atmosphere and without any washing procedure to eliminate electrolyte residuals.

As anticipated in the previous report, for the 50 nm Si + 3 nm $SiO_2$ an interesting finding is shown by the ATR-FTIR spectra reported in Fig. 1 (a-b). In the C-O and C=O bond region (Fig.1 (a)), the comparison with the reference spectra of the dried electrolyte (obtained as a result of the evaporation of EMC), clearly indicates that most of the contributes can be related to electrolyte residuals. However, in the spectra of the fully lithiated electrode (0.05V) new contributes appear, which are assigned to the appearance of LiEDC as decomposition product of EC.[4] Interestingly these contributes disappear upon further de-lithiation.

As highlighted in the previous report the study, conducted also upon further cycles (data not shown here), represents a fundamental observation for the understanding of the SEI stability of silicon electrodes. Indeed, the disappearance of LiEDC is not related to its solubility, as proved by washing the electrodes with DEC. Indeed, even after the rinsing step the LiEDC peaks are still present, thus suggesting the disappearance of LiEDC to be related either to a mechanical detachment from the silicon surface or the possible oxidation upon further de-lithiation. The same behavior is observed for the second SEISta model electrode, i.e. 50 nm Si + 10 nm $SiO_2$. LiEDC appears at fully lithiated state and subsequently disappears upon oxidation as reported in Fig. 1 (c).

Despite the two model systems present comparable FTIR features within the 1100-2000 $cm^{-1}$ spectral region, some differences are observed at low frequency values, generally dominated by features related to P-F bond containing compounds and possible silicate formation. For the silicon thin film with the native oxide layer, an accumulation of P-F containing species is observed upon cycling and most likely related to the decomposition of the $LiPF_6$ salt.[5] Indeed, by performing the same study with a $LiPF_6$ free electrolyte, i.e. 1.2M LiTFSI EC:EMC 3:7 wt.%, the PF containing compounds are not detected. Interestingly, upon de-lithiation, the intensity of the broad band at about 840 $cm^{-1}$ decreases again, together with the new features observed at 800 $cm^{-1}$ and 1050 $cm^{-1}$ (see Fig. 1 (b)). For the model electrodes with a thicker oxide layer, a comparable presence of P-F containing species is observed, however new peaks at about 1037 $cm^{-1}$ are detected starting at 0.5 V till the fully lithiated state, to then disappear again during the de-lithiation process. The new features may be related to the presence of other electrolyte decomposition products, such as DEDOHC [6], or the eventual presence of non-stoichiometric silicates. Work toward the identification and assignment of these features is still in progress.

The results herein discussed represents a step forward the understanding of the stability of the silicon electrolyte interphase. The accumulation and following disappearance of different species on the electrode's surface, clearly suggest a dynamic SEI formation and "dissolution". The "breathing" mode of the passivating layer on top of the silicon thin films has been also detected by X-ray absorption spectroscopy. The analysis of the Silicon L-edge (Fig. 1(e)) reveals the formation and thickening of a surface layer upon lithiation, which upon de-lithiation reduces considerably its thickness, thus further confirming the dynamic growth and disappearance of the surface layer.
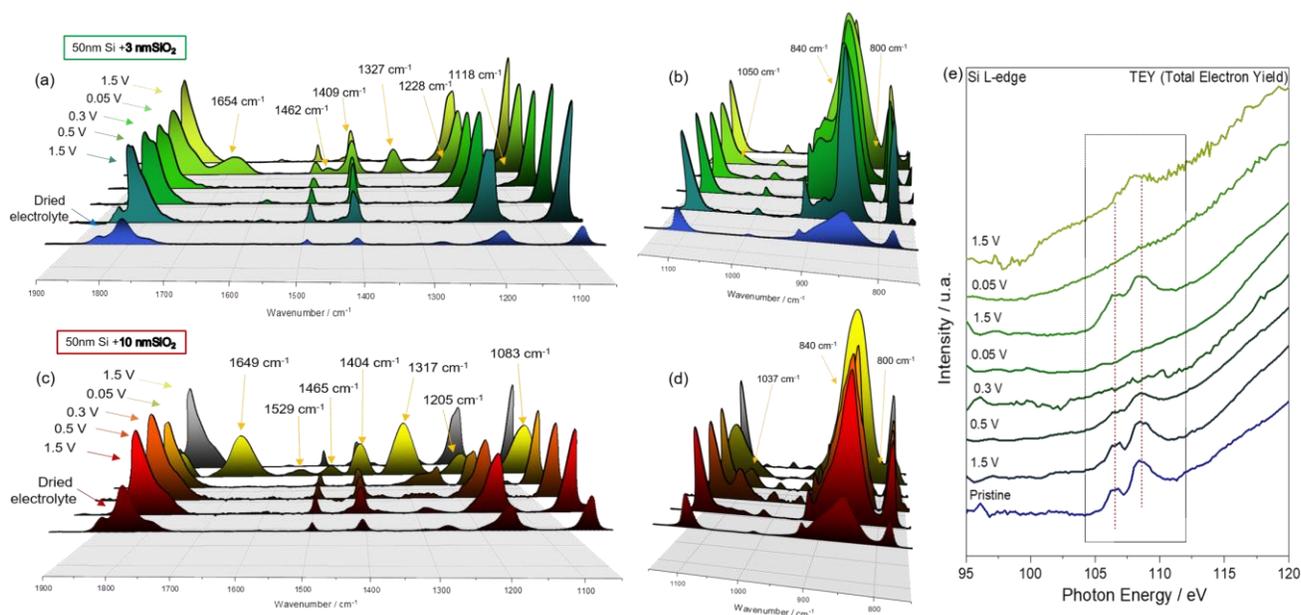


Figure 1. Ex-situ ATR-FTIR spectra at different state of charge for the (a, b) 50 nm Si thin films with native oxide layer and (c, d) 50 nm Si+10 nm $SiO_2$ electrode. (e) Ex-situ XAS analysis at the Si L-edge collected in TEY mode for the 50 nm Si thin film with native oxide.

## Conclusions

Characterization in terms of electrochemistry, FTIR and XAS of the silicon electrolyte interphase formation on the Si thin film SEISta model samples, with and without sputtered oxides overlayers, has been completed.

The results indicate, for all the investigated samples, a dynamic growth and disappearance of the passivating surface film, thus suggesting the oxide layer does not affect the interfacial chemistry significantly. This fundamental observation represents a step forward the understanding of the inherent non passivating behavior of silicon electrodes. A qualitative detection of the chemical compounds most likely responsible of the "breathing" effect of the surface film has been successfully reached, thus enabling the correlation of the formation and disappearance of LiEDC, but also to P-F containing species, to the stability of the SEI .
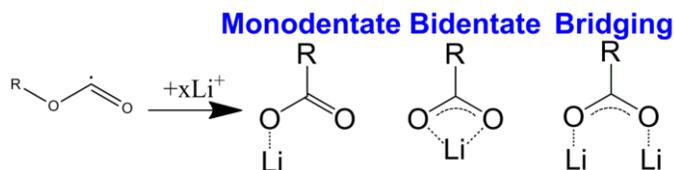
## References

[1] E. Peled, *J. Electrochem. Soc.*, **126**, 2047-2051 (1979).

[2] M. Winter, *Zeitschrift Für Phys. Chemie.*, **223**, 1395-1406 (2009).

[3] M.N. Obrovac, V.L. Chevrier, *Chem. Rev.*, **114**, 11444-11502 (2014).

[4] G.V. Zhuang, K. Xu, H. Yang, T. R. Jow, P.N. Ross, *J. Phys. Chem. B*, **109**, 17567-17573 (2005).

[5] G.M. Veith, M. Doucet, R.L. Sacci, B. Vacaliuc, J.K. Baldwin, J.F. Browning, *Sci. Rep.,* 7, 6326, (2017).

[6] F. Shi, P.N. Ross, G.A. Somorjai, K. Komvopoulos, *J. Phys. Chem. C*,**121**, 14476-14483 (2017).

## SEI Characterization: In Situ Study Of SEI Formation as an Effect of Polymeric Binders

### Guang Yang, (ORNL) and Jagjit Nanda (ORNL)

## Background

In last two reports, we studied the chemical signature of the SEI from the TERS measurements and analyzed the evolution of SEI in model amorphous Si (a-Si) as a function of cycling (1X, 5X and 20X, X denotes the cycle numbers). Our key findings show that for 1X cycled a-Si, has local SEI species containing poly (ethylene oxide) (PEO) - like oligomer and lithium ethylene dicarbonate (LEDC, $(CH_2OCOOLi)_2$), whereas the SEI on 5X a-Si is more dominated by the LEDC species.  On the other hand, SEI on 20x a-Si is enriched with carboxylate compounds. Detailed TERS investigation show that for 20X a-Si, there are indications that carboxylate compounds have different conformations with respect to coordination of $Li^+$ cation (see Scheme I).



**Scheme I. Scheme of possible reaction path to form the various carboxylate conformers on 20x a-Si**

## Results

50 nm thick a-Si was sputtered on a copper electron collector at ORNL and cycled as per the procedure finalized by the round robin team of SEIsta. TERS experiments were performed using a HORIBA Xplora Nano Raman Platform integrated with AIST-NT SPM system (laser wavelength = 532 nm and the objective was 100x, 0.7 N.A.) The laser power was set at 25 µW. The TERS tip was fabricated by thermal evaporating 2 nm chromium on commercial Bruker silicon tip (26 N/m, 300 kHz), followed by coating a 40 nm silver layer. All TERS measurements were performed in a special Ar-compatible antechamber to avoid air exposure. Theoretical Raman spectra were calculated using cluster-based DFT calculations for comparison within the Gaussian (G16)[1] suite of programs. Becke's three-parameter hybrid method using the Lee–Yang–Parr correlation functional (B3LYP)[2] was chosen for this study. The DFT simulation was supported by Tingzheng Hou and Dr. Kristin Persson.
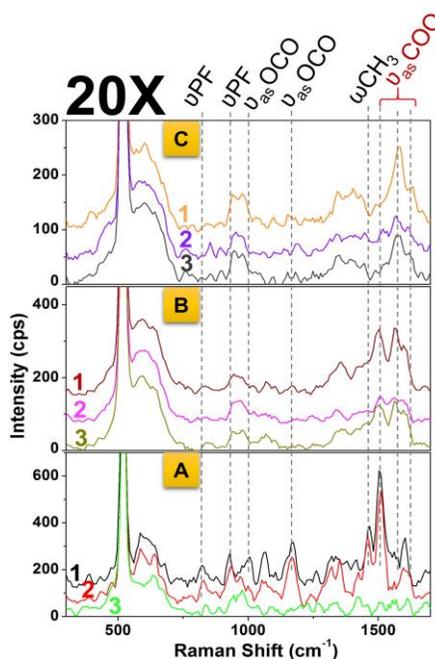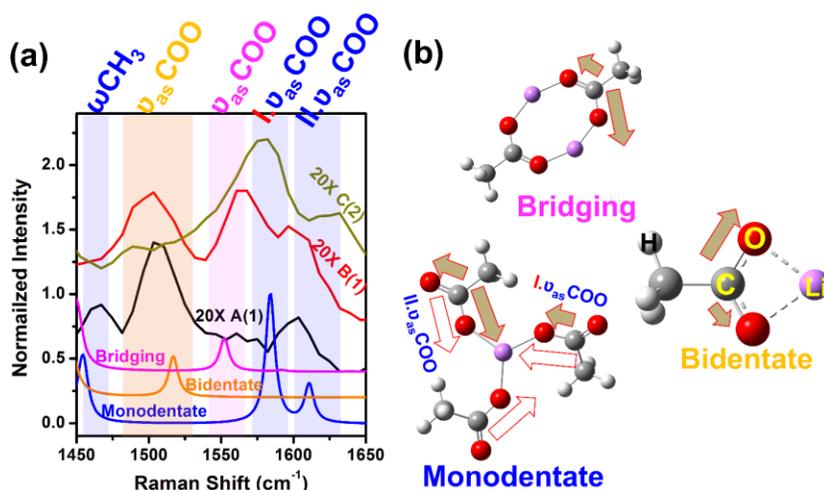


**Figure 1. TERS spectra of collected from various locations of 20X a-Si. The Greek symbols denote corresponding vibrational modes for ν, stretching and ω, wagging.**

Figure 1 shows various TERS spectra taken from 20X a-Si surface. An immediate observation is that several vibrational modes between 1450 cm$^{-1}$ and 1650 cm$^{-1}$ gain in intensity, which cannot be assigned to either PEO or LEDC, These bands are most likely ascribed to various carboxylate compounds (RCO$_2$Li),[3] which are formed either by thermal decomposition of the LEDC per prolonged galvanostatic cycling[4] or by ester radicals coordinating to Li$^+$ (Scheme I).[5] Interestingly, although studied by several groups using traditional IR spectroscopy,[4, 6-7] the vibrational bands related to carboxylates on Si anode were not precisely resolved and explained in detail, possibly due to the low IR absorbance of related bands in this frequency region. Detailed comparison of the experimental TERS spectra taken from various locations from 20X a-Si and those calculated by DFT calculations of three different carboxylate conformations is shown in Figure 2. The TERS spectrum taken from Region A, Spot 1 (denoted as 20X A(1), TERS mapping is not shown here) has a featured band at 1511 cm$^{-1}$ and a satellite band at 1460 cm$^{-1}$, in accordance with the asymmetric -COO stretching mode from the bidentate carboxylate (ca. 1517 cm$^{-1}$) and the CH$_3$ wagging mode from the monodentate carboxylate (ca. 1454 cm$^{-1}$), respectively (Figure 2(b)).[3] The analysis on the bands of lower frequencies indicate the acetate ions are less coordinated to Li$^+$ cation. For Spectrum 20X B(1), the broad peak centered at 1565 cm$^{-1}$ may be ascribed to the convolution of asymmetric -COO stretching band of the

bridging confirmation (ca. 1552 cm$^{-1}$) and asymmetric -COO stretching band of the monodentate (ca. 1584 cm$^{-1}$) based on the calculation results. The Spectrum 20X C(2) has two distinguished bands at 1581 cm$^{-1}$ and 1632 cm$^{-1}$. Both of them are ascribed to the monodentate asymmetric -COO stretching mode. The calculated spectra indicates that the lower frequency band stems from the asymmetric movement of the coordinated (with Li$^+$) oxygen towards the central Li$^+$ (denoted as I.$v_{asCOO}$, golden arrows) whereas the higher frequency band is ascribed to the symmetric movement of the surrounding oxygen oscillates towards the central Li$^+$ (denoted as II.$v_{asCOO}$, red arrows). The subtle difference of these two vibrational modes is illustrated in Figure 2(b). Hence, based on the above comparison and analysis, it is evident that TERS is uniquely capable of depicting the conformational change of the carboxylate compounds of nanometer resolution, which cannot be acquired by bulk spectroscopy, such as IR.

**Figure 2. (a) Comparison between normalized TERS spectra taken from various locations of the 20X a-Si surface and simulated counterparts. (b) Three conformations of the carboxylate compounds coordinated with Li+. Arrows indicate -COO asymmetric stretching modes for monodentate, bidentate and bridging conformations, respectively.**



## Conclusions

Detailed TERS investigation show that for 20X a-Si, there are indications that carboxylate compounds have different conformations with respect to coordination of Li$^+$ cation. These conformations are spatially heterogenous at the nanoscale. We further verify that the TERS spectra collected from various locations on 20X a-Si are in good agreement with the theoretical Raman spectra using different carboxylate conformer models, calculated using density functional theory (DFT).

## References

1.    Frisch, M. J.; Trucks, G. W., et al. *Gaussian 16 Rev. A.03*, Wallingford, CT, 2016.

2.    Becke, A. D., Density-functional thermochemistry. III. The role of exact exchange. *The Journal of Chemical Physics* **1993,** *98* (7), 5648-5652.

3.      Socrates, G., *Infrared and Raman characteristic group frequencies: tables and charts*. John Wiley & Sons: 2001.

4.      Yoon, T.; Milien, M. S.; Parimalam, B. S.; Lucht, B. L., Thermal Decomposition of the Solid Electrolyte Interphase (SEI) on Silicon Electrodes for Lithium Ion Batteries. *Chem. Mater.* **2017,** *29* (7), 3237-3245.

5.      Schroder, K. W.; Celio, H.; Webb, L. J.; Stevenson, K. J., Examining Solid Electrolyte Interphase Formation on Crystalline Silicon Electrodes: Influence of Electrochemical Preparation and Ambient Exposure Conditions. *J. Phys. Chem. C* **2012,** *116* (37), 19737-19747.

6.      Nie, M.; Abraham, D. P.; Chen, Y.; Bose, A.; Lucht, B. L., Silicon solid electrolyte interphase (SEI) of lithium ion battery characterized by microscopy and spectroscopy. *J. Phys. Chem. C* **2013,** *117* (26), 13403-13412.

7.      Shi, F.; Ross, P. N.; Somorjai, G. A.; Komvopoulos, K., The Chemistry of Electrolyte Reduction on Silicon Electrodes Revealed by in Situ ATR-FTIR Spectroscopy. *J. Phys. Chem. C* **2017,** *121* (27), 14476-14483.